Journal of Advanced Research 30 (2021) 197–211

Contents lists available at ScienceDirect

Journal of Advanced Research

journal homepage: www.elsevier.com/locate/jare

PAP90, a novel rice protein plays a critical role in regulation of D1 protein stability of PSII

M. Raghurami Reddy [a], Satendra K. Mangrauthia [a,*], S. Venkata Reddy [c], P. Manimaran [c], Poli Yugandhar [b], P. Naresh Babu [a], T. Vishnukiran [b], D. Subrahmanyam [b], R.M. Sundaram [a], S.M. Balachandran [a,*]

[a] Biotechnology Laboratory, Crop Improvement Section, ICAR-Indian Institute of Rice Research, Rajendranagar, Hyderabad 500030, India
[b] Physiology Laboratory, Crop Production Section, ICAR-Indian Institute of Rice Research, Rajendranagar, Hyderabad 500030, India
[c] Department of Plant Sciences, University of Hyderabad, Hyderabad 500046, India

GRAPHICAL ABSTRACT

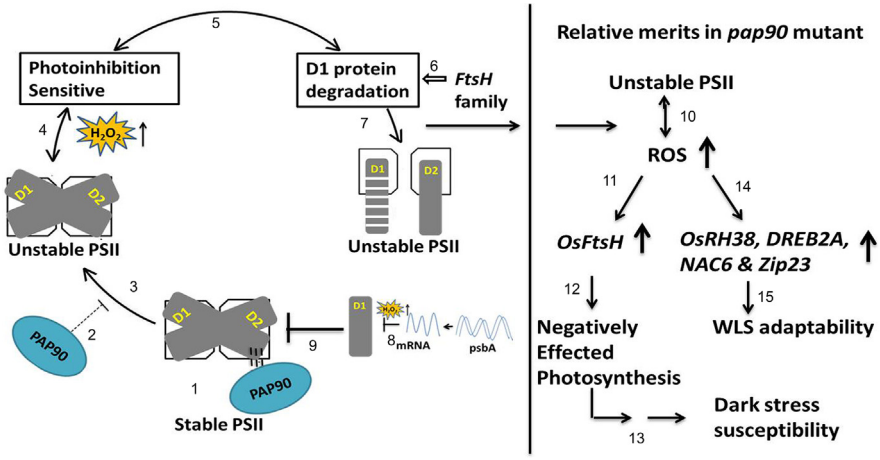

ARTICLE INFO

Article history:
Received 8 July 2020
Revised 29 October 2020
Accepted 17 November 2020
Available online 23 November 2020

Keywords:
Abiotic stress
D1 protein
Oryza sativa L.
OsFtsH
Photosystem II
ROS

ABSTRACT

Introduction: Photosystem II (PSII) protein complex plays an essential role in the entire photosynthesis process. Various known and unknown protein factors are involved in the dynamics of the PSII complex that need to be characterized in crop plants for enhancing photosynthesis efficiency and productivity.
Objectives: The experiments were conducted to decipher the regulatory proteins involved in PSII dynamics of rice crop.
Methods: A novel rice regulatory protein PAP90 (PSII auxiliary protein ~90 kDa) was characterized by generating a loss-of-function mutant *pap90*. The mutation was characterized at molecular level followed by various experiments to analyze the morphological, physiological and biochemical processes of mutant under control and abiotic stresses.
Results: The *pap90* mutant showed reduced photosynthesis due to D1 protein instability that subsequently causes inadequate accumulation of thylakoid membrane complexes, especially PSII and decreases PSII functional efficiency. Expression of *OsFtsH* family genes and proteins were induced in the mutant, which are known to play a key role in D1 protein degradation and turnover. The reduced D1 protein accumulation in the mutant increased the production of reactive oxygen species (ROS).

Peer review under responsibility of Cairo University.
* Corresponding authors.
E-mail addresses: Satendra.KM@icar.gov.in (S.K. Mangrauthia), balasena@yahoo.com (S.M. Balachandran).

https://doi.org/10.1016/j.jare.2020.11.008
2090-1232/© 2020 The Authors. Published by Elsevier B.V. on behalf of Cairo University.
This is an open access article under the CC BY-NC-ND license (http://creativecommons.org/licenses/by-nc-nd/4.0/).

The accumulation of ROS along with the increased activity of antioxidant enzymes and induced expression of stress-associated genes and proteins in *pap90* mutant contributed to its water-limited stress tolerance ability.

Conclusion: We propose that PAP90 is a key auxiliary protein that interacts with D1 protein and maintains its stability, thereby promoting subsequent assembly of the PSII and associated membrane complexes.

© 2020 The Authors. Published by Elsevier B.V. on behalf of Cairo University. This is an open access article under the CC BY-NC-ND license (http://creativecommons.org/licenses/by-nc-nd/4.0/).

Introduction

Analysis of genetic mutations is an effective method to characterize the incognito genes in functional genomics. Among various mutagenesis approaches, loss-of-function is a good approach to discover rice genes and their biological significance [1]. The loss-of-function mutant population can be generated by several mutagens including insertional mutagenesis by T-DNA [2] or mobile genetic elements [3]. The global objectives of these studies are to enrich the gene resources, which can further be used in crop improvement in terms of yield, stress tolerance, and other useful agronomic traits. The performance of a crop mainly depends on the photosynthesis efficiency that plays a pivotal role in the conversion of light energy into chemical energy and stores it for future use [4].

Photosynthesis is processed by integral membrane protein complexes that include PSII, Cytochrome b6f complex, Photosystem I (PSI), and F-ATPase on thylakoid membrane of chloroplast [5]. Various studies revealed that the formation and maintenance of dynamics of these functional photosynthetic complexes is a multistep process [6]. Numerous characterized and uncharacterized proteins play critical roles in regulating these processes directly or indirectly [7]. The PSII is a multi-subunit protein complex formed with 27–28 subunits [8]. The biogenesis of PSII starts with the formation of reaction center by two homologous proteins D1 and D2, and two other closely related chlorophyll (chl) coordinating proteins (CPs), CP43 and CP47 along with Cytochrome *b* complex [9]. The dimerization of PSII monomers and association with trimeric LHCII completes the formation of PSII complex [6].

Several auxiliary or regulatory proteins are involved in the assembly and maintenance of stoichiometry of PSII complex at various levels viz. ALB3, HCF136, and HCF243 in *Arabidopsis*. The *ALB3* gene is mainly involved in integration of thylakoid membrane integral proteins, especially insertion of D1 protein into PSII [10]. The HCF136 interacts with D2 protein during the formation of reaction center [11]. Functional reduction of *HCF136* gene failed to form the functional PSII complex although the complex associated proteins were synthesized [12]. The HCF243 specifically interacts with D1 protein of PSII and maintains its stability. The loss-of-function of *HCF243* gene causes instability of D1 protein and inadequate accumulation of PSII supercomplexes [13]. These factors regulate the PSII by interacting with core subunits or complexes. Most of these studies about PSII regulatory factors and their interactions are reported in *Arabidopsis* [11,13]. Although many homologues of these regulatory factors have also been identified in rice, functional characterization of these genes is yet to be validated. Overall, the absence of important regulatory proteins negatively affects the PSII efficiency either directly or indirectly, and thus led to enhanced photoinhibition and photooxidative damage [14]. In addition, PSII is primary target under various abiotic stresses, especially, light induced stress that directly inactivates the PSII through photoinhibition [15]. The photodamaged PSII produces reactive oxygen species (ROS), which act as the secondary signaling molecules in stress response. Other abiotic stresses indirectly affect the PSII by generating ROS which inhibits the PSII repair cycle, particularly de novo synthesis of D1 protein [15].

The photodamage of PSII mainly affects the D1 protein and hence, the repair needs rapid synthesis and replacement of the D1 proteins, encoded by *psbA* gene [16]. In PSII repair cycle, D1 protein turnover is associated with removal of the proteolytically cleaved D1 proteins by ATP-dependent zinc metalloproteases (FtsH), and integration of newly synthesized D1 proteins into the thylakoid membrane [17]. In rice, nine FtsH proteins (*OsFtsH1* to *OsFtsH9)* have been identified so far [18]. In *Arabidopsis*, 12 *FtsH* genes were identified and each gene showed homology with the corresponding *OsFtsH* genes of rice, except *FtsH*9 and *12* [18]. Most of these gene products are localized in chloroplast or mitochondria and associate with D1 protein turnover [19].

In this study, we developed and characterized the *pap90* rice mutant that showed reduced functional efficiency of PSII due to negative regulation of D1 protein stability and function. Biochemical analysis of mutant revealed up-regulation of OsFtsH family genes and physical interaction of PAP90 with D1 protein of PSII. The introgression of WT-*OsPAP90* gene into mutant plants restored the WT phenotype in F1 recombinants. Based on the evidence, we propose that the nuclear-encoded PAP90 plays an important role in stabilizing the D1 protein. The loss-of-function of *OsPAP90* gene resulted in the accumulation of ROS in mutant and subsequent adaptations contributed to its water-limited stress (WLS) tolerance ability and dark stress susceptibility.

Materials and methods

Mutant development and molecular analysis

The T-DNA of En-Bar construct carried tetrameric (4X) enhancer element derived from the cauliflower mosaic virus (CaMV) 35S promoter (domain B: −343 to −46) [20] along with *bar* gene (phosphinothricin acetyltransferase) that confers resistance to phosphinothricin (Fig. 1A). Three-week-old embryogenic calli from the rice cv BPT 5204 were used as the explant for *Agrobacterium*-mediated transformation as described earlier [21]. The untransformed wild-type (WT) and transformed plants were maintained in a biosafety glasshouse under control conditions.

The integrated T-DNA was confirmed through PCR of *bar* gene cassette using specific primers (F:5′-CAAAGGGTAATATCGGGAAACC-3′; R:5′-TCAGCAGGTGGGTGTAGA-3′) as described previously [22]. Further, PCR positive transgenic plants were confirmed through Southern hybridization. Here, *EcoRI* and *XhoI* restriction enzymes were used for the DNA (~15 μg) fragmentation. Mobilization onto Hybond-N + membrane (GE Health Care Ltd., UK) followed by UV cross-linking (700 kJ for 3–5 min), probe preparation, hybridization, stringency washes, and signal detection were performed as per the manufacture's instructions using the ready-to-go-labeling kit (GE Health Care Ltd., UK). The 686 bp fragment spanning CaMV 35S promoter and a *bar* gene was used as a probe.

Thermal Asymmetric Interlaced Polymerase Chain Reaction (TAIL-PCR) was performed to identify the T-DNA integration locus by analyzing the flanking sequences, as described [23] with minor modifications. Freshly isolated genomic DNA of *pap90* mutant was used as an initial template in primary PCR reactions. A total of

three subsequent PCR reactions were carried with a common arbitrary degenerate primer (AD) and four nested primers targeting the 3′ end of the *bar* gene cassette for the identification of left border flanking sequences. The diluted (1:100) primary PCR product was used as a template for the secondary reaction. Further, in a tertiary PCR reaction, 1:10 diluted secondary PCR product was used as a template. The tertiary PCR reaction was carried out with two different nested primers individually for accuracy. The details of reaction setup, PCR profile, and nested primers are listed in Supplementary Tables S1-S3. The tertiary PCR products were purified (Wizard ® SV Gel and PCR Clean-Up System, Promega, USA) followed by sequencing (Sandor Lifesciences, India). The sequenced data was analyzed through BLAST at the rice annotation project database (RAP-DB) [24].

Gene expression and proteomic studies

Gene expressions were analyzed through semi-quantitative reverse transcription PCR (semi-qRT-PCR) and real-time or quantitative PCR (qPCR) at transcript levels. Total RNA was extracted from 100 mg of freshly collected rice flag leaves using Nucleospin RNA Plant Kit (Macherey Nagel, Germany) and used as a template for cDNA synthesis using PrimeScript First Strand cDNA Synthesis Kit (Takara, Japan). The normalized cDNA was used for both semi-qRT-PCR and qPCR reactions with gene-specific primers. Semi-qRT-PCR was performed with the standard protocol as described [25]. *OsActin* was used as internal control. The qPCR reaction was prepared by mixing the cDNA with 10 μl of 2X SYBR premix (Takara, Japan), 2 μM each of gene-specific primers in 20 μl reaction volume. The PCR profile for qPCR was as follows: initially at 95 °C for 10 min followed by 35 cycles at 95 °C for 15 s, 58 °C for 15 s, and 72 °C for 10 s, followed by melting curve analysis. The reaction was run in 96-well optical reaction plate (Roche Light cycler, Switzerland). Based on Ct values, the gene expression variations in terms of fold change was calculated by using the $2^{-\Delta\Delta Ct}$ method [26]. The standard deviations of ΔC_T values were calculated as described [27]. *OsActin* was used as internal control. The fold change mean values were obtained from three biological replicates. The primers used for both semi-qRT-PCR and qPCR are listed in Supplementary Table S4, S6.

The proteomic studies were carried out by 2D gel electrophoresis (2DE), Western blotting, blue native-SDS PAGE (BN-SDS PAGE), and yeast two-hybrid (Y2H). The protein extraction from rice flag leaves and 2DE was performed as described [28]. The first dimension run was performed using 125 μg of each protein sample at 20 °C in the PROTEAN IEF focusing tray. Further, IPG strips (pH 4–7) were equilibrated, and a second-dimensional run was carried out at 20 mA for 6 h followed by staining and de-staining (SE600 Vertical Unit-GE Healthcare). By using GE image scanner, the differentially expressed protein spots were identified and analysed through Matrix-Assisted Lazer Desorption/ Ionization–Time of Flight Mass Spectrometry (MALDI-ToF/MS) (Sandor Proteomics, India). The resulted protein data was analysed in MASCOT/MS peptide search engine (Supplementary Table S5).

For Western Blotting, 100 mg of flag leaf was homogenized with 1.0 ml of chilled protein extraction buffer (50 mM Tris-HCl: pH 7.4; 1 mM EDTA; 2 mM $MgCl_2$; 2 mM DTT; 2.5 mM PMSF and 0.1% Triton-X-100) followed by centrifugation at 15,000 g for 10 min at 4 °C. The collected supernatant was diluted to 10% final concentration with 100% TCA and incubated at −80 °C for overnight. In continuation, the incubated samples were centrifuged at 15,000 g for 15 min at 4 °C and discarded the supernatant. Further, the pellet was washed thrice with cold acetone followed by vacuum drying. The pellet was solubilized in a sample buffer (8.0 M urea; 2% CHAPS; 50 mM DTT) and the protein concentrations were estimated by Bradford protein assay [29]. Nearly 75 μg of rice flag leaf protein samples from both WT and *pap90* mutant were resolved on 11% SDS-PAGE followed by transferring on to the nitrocellulose membrane (Millipore, USA) by using Bio-Rad Western apparatus. The membrane was blocked with 5% non-fat milk in tris-buffered saline, pH 7.4 (TBS) + 0.1% Tween-20 for 1 h at RT. Then the membrane was incubated with a primary antibody, anti-D1 protein antibody (Agrisera, Sweden) prepared in TBS-T (TBS + 0.1% Tween-20) with 1:10000 dilution of 2% BSA and incubated overnight with constant shaking at 4 °C. After three washes with TBS-T solution, conjugated with diluted (1:20000 in TBS-T + 2% BSA) anti-Rabbit HRP secondary antibody (GE health care life Sciences, USA), and incubated for 2 h at RT. After 3 washes with TBS, ECL substrate (Femtolucent Plus-HRP, chemiluminescent reagent from Bio-Rad, USA) was added to the membranes and the blot was scanned for chemiluminescence using Versadoc (Bio-Rad, USA) molecular imager to capture the signal intensity.

The thylakoid membrane complexes were analyzed through BN-SDS PAGE. The chloroplast were isolated from fresh rice flag leaves and 125 μg of chl was used as starting material to solubilize the thylakoid membrane complexes in buffer (2% DDM solution was used to solubilize the membrane complexes) [30]. These complexes were analyzed through BN-SDS PAGE by resolving on non-gradient (separating gel: 8% acrylamide and stacking gel: 4% acrylamide) and gradient gels (separating gel: 6–12% acrylamide and stacking gel: 4% acrylamide). The electrophoretic separations of complexes were carried at 4 °C, and the protein complexes were visualized directly in the BN-SDS PAGE and also stained with Coomassie blue dye.

Y2H assay was performed to identify the interaction between PAP90 and D1 proteins. The complete CDSs of PAP90 and D1 was cloned into pGBKT7 (BD) and pGADT7 (AD) vectors, respectively, and vice-versa. The recombinant BD and AD vectors were transformed into two individual mating yeast strains viz. Y2HGold and Y187, respectively. The mating experiments followed plating on minimal, synthetically defined (SD) medium plates devoid of leucine and tryptophan (SD-Leu-Trp: double dropout-DDO) as per manufacturer's instructions (Matchmaker Gold Yeast Two-Hybrid System, Clontech). Further, the mated cells were screened on SD-Leu-Trp-His (triple drop out-TDO) and SD-Leu-Trp-His-Ade (Quadruple dropout-QDO) medium to find the interaction between PAP90 and D1 proteins. The ability of mated cell's growth on TDO and QDO medium within 3–5 d, confirmed the interaction between the PAP90 and D1 proteins. The mated culture of BD-p53/AD-T antigen (known interaction) and BD-lamin/AD-T antigen (no interaction) were used as positive and negative controls, respectively.

Physiological analysis

Infra-Red Gas Analyzer (IRGA) associated fluorometer (LCF Model 6400–1, LICOR, USA) system was used to measure the gas exchange parameters viz., P_N (net photosynthesis rate), g_s (stomatal conductance), E (transpiration rate), C_i (intercellular CO_2 concentration), WUE (P_N/E -water use efficiency) and iWUE (P_N /g_s - intrinsic water use efficiency) under both control and stress conditions (10 d after the commencement of WLS). During these studies, photosynthetic photon flux density (PPFD) and CO_2 concentration were kept at 1200 μmol m^{-2} s^{-1} and 387 ± 6 ppm, respectively.

The total chl and relative water content (RWC) were estimated in both WT and mutant as described [31,32], respectively. The mean values obtained from three biological replicates were presented.

Further, the chl fluorescence studies were carried on 30 min dark-adapted leaves of both *pap90* mutant and WT with the aid of a portable fluorometer [PAM-210 (Pulse amplitude modulation) Walz, Effeltrich, Germany]. The Fo (minimal fluorescence yield); Fm (maximal fluorescence yield); Fv/Fm [maximum quantum effi-

ciency of PSII is the ratio of Fv (maximum variable fluorescence) to Fm, Fv/Fm= (Fm-Fo)/Fm]; Ft (fluorescence yield); Fm' (maximal fluorescence yield); ETR (electron transport rate); qP (coefficient of photochemical quenching); qN (coefficient of non-photochemical quenching); and ϕPSII (effective PSII quantum yield) were measured as described [33]. The mean values obtained from three biological replicates were presented.

Biochemical analysis

The histochemical staining of superoxide (O_2^-) radicals, and hydrogen peroxide (H_2O_2) was performed in the leaf samples as described [34]. The O_2^- superoxide radicals and H_2O_2 were detected by staining with a fresh nitroblue tetrazolium (NBT) and 3,3'-diaminobenzidine (DAB) solutions, respectively. Blue color spots were observed due to the formation of the precipitate at the site where NBT interacted with O_2^-. H_2O_2 was visualized in the form of brown spots which were the polymerized product of DAB. In addition, H_2O_2 was quantified as described by Alexieva et al (2001) [35]. The reaction mixture consisted 0.5 ml supernatant of leaf extract, equal amount of 10 mM phosphate buffer (pH 7.0), and 2 ml of 1 M freshly prepared potassium iodide (KI). The reaction mixtures were incubated in dark for 30 min and measured the absorbance at 390 nm. The amount of H_2O_2 in WT and *pap90* mutant were calculated based on standard curve prepared with known H_2O_2 concentrations. The H_2O_2 quantity was expressed in μmol g^{-1}FW. The presented mean values were obtained from three biological replicates.

Malondialdehyde (MDA) is a byproduct of lipid peroxidation indicating the membrane damage and measured in both *pap90* mutant and WT as described [36]. Antioxidant enzyme assays for SOD [37], CAT [38], and POD [39] were performed as described. The enzyme activity was expressed in unit mg^{-1} protein.

Proline [40], total soluble sugars (TSS) and starch content [41] were determined in flag leaves of both WT and *pap90* mutant as described. In all these experiments, the presented mean values were obtained from three biological replicates.

Electron microscopic studies

The flag leaves from WT and mutant were observed under a scanning electron microscope (SEM) and transmission electron microscope (TEM). The grids were prepared by using an automated sputter coater (Model: JEOL-JFC-1600) and observed under SEM (Model: JOEL-JSM-5600) at suitable magnifications. For TEM, the leaf samples (0.5x0.5 mm^3) sections were carried out with ultra-microtome (Leica ultra-cut UCT-GAD/E-100, Germany). These sections were observed under TEM (H-7500, Hitachi, Japan) [42].

In-silico analysis

We analyzed PAP90 sequence in various bioinformatics online tools like SMART, CDD, InterPro, Pfam, and HHPred for the information about gene family. The phylogenetic tree was constructed through PhylomeDB [43]. In the constructed tree (Supplementary Figure S3), blue and red boxes indicate the speciation and duplication events, respectively. The green circle indicates the target sequence (PAP90). In addition, the homologous protein sequences from different species were obtained from NCBI/UniProt. The multiple sequence alignment was performed through ClustalW/BLASTP to identify the sequence/domain similarity. The PAP90 protein interaction network was predicted through online tool 'STRING' [44]. To analyze the *cis*-regulatory elements of *OsPAP90* gene, 1.5 kb upstream region was retrieved from RAP-DB. The *cis*-regulatory elements were identified from the sequence by using an online tool- 'Plant Care' [45].

Various stress treatments

Two-week-old rice seedlings were grown hydroponically on the Yoshida medium at 28 ± 2 °C [41] followed by various treatments. For osmotic and salt (NaCl) stresses, the Yoshida solution was supplemented with 15% polyethylene glycol (PEG 6000) and 200 mM NaCl, respectively. For hormone treatment, 100 μM abscisic acid (ABA) was used as a final concentration. The dark stress was imposed to plantlets by maintaining complete dark condition at 28 ± 2 °C. The duration of all abiotic stress treatment was 24 h in hydroponics.

Screening against WLS: two weeks old plants were transferred into ten earthen pots (twenty plants, two plants per pot) and maintained in biosafety greenhouse as two sets (temperature 32 ± 2 °C, relative humidity 55 ± 5%). For the first two weeks, plants (both set I and set II) were maintained with an ample amount of water in the pots (3–4 cm overlay of water above the soil level). The water surface was fully overlaid with polystyrene balls to prevent evaporation. After two weeks, water stress was commenced by restricting the water completely for six days and later to maintain the minimum moisture condition in set I. But, set II was maintained with an ample amount of water throughout the experiment and considered as controls. Following the commencement of water stress, symptoms like wilting and drying of leaf tips were observed after 10–12 d in WT and 18–21 d in mutants.

Screening against dark stress: two weeks old plantlets from mutant and WT in Yoshida medium were used to screen against dark stress by incubating in complete dark condition at 28 ± 2 °C. The Yoshida solution was replaced with fresh solution for every 72 h. After the commencement of dark stress, photosynthesis associated genes [46] expression studies were carried in mutant and WT at various time points viz. 24, 48, and 72 h as described above. Further, treatment was prolonged up to 15 d to observe the mutant phenotypic variance like chlorosis rate at regular time intervals.

Yield associated traits

The data viz. plant height, total number of tillers, number of panicles, panicle length, number of grains per panicle, and grain yield per plant were collected from both *pap90* mutant and WT plants (n = 16).

Restoration of OsPAP90 gene expression through crossing

The crossings were performed between the *pap90* mutant and WT plants. The WT and *pap90* were considered homozygous dominant and recessive parents for *OsPAP90* gene, respectively. The obtained F_1 recombinants (*pap90* X WT) are heterozygous for *OsPAP90* gene. Phenotypic variations viz. flag leaf length and width were observed and the differences were measured from three independent plants in duplicates by using the ImageJ tool. Simultaneously, the *OsPAP90* gene expression was analyzed in both parents and recombinants through qPCR using three biological replicates.

Statistical analysis

The statistical significance of experimental data from the mean of biological replicates with standard error (SE) was analyzed through a student's *t*-test at $P < 0.05$ (*statistically significant), $P < 0.01$ (**very statistically significant) and $P < 0.001$ (***extremely statistically significant). Analysis of variance (ANOVA) was performed through Statistix Ver 8.1 and mean values significance was calculated by the least significant difference (LSD) test (alpha at 0.05).

Results

Development and identification of pap90 rice mutant

About 133 activation tagged mutant lines of indica rice cv. BPT 5204 were developed by using En-Bar construct. The developed mutant population is predominant resource for functional genomics. The mutants were primarily screened based on phenotypic and morphological variations with WT followed by molecular and functional characterization. Upon screening, we identified one of the mutants (*pap90*) restricted its phenotypic inequalities to homozygous recessive condition. The observed phenotype and preliminary molecular and physiological data prompted us to select the *pap90* mutant for this study. The selected mutant was advanced and further confirmed the T-DNA insertion in subsequent generations through PCR and Southern hybridization (Fig. 1A). In continuation, TAIL-PCR results revealed that the T-DNA was integrated at 1.8 kb downstream from the start codon of *OsPAP90* (LOC_Os06g24540) gene encoding a conserved hypothetical protein (PAP90) (Fig. 1B, C) (Supplementary Table S1-S3). The disruption of *OsPAP90* expression by T-DNA integration was confirmed by qPCR and semi-qRT-PCR (Fig. 1D, E) (Supplementary Table S4). Also, we sought to exclude the possibility of off-target effects of the 4X enhancer of T-DNA on the expression of nearby genes within 50 kb flanking region from integration site. A histone mRNA exonuclease 1 (LOC_Os06g24594) and another hypothetical protein of DUF679 family (LOC_Os06g24490) were located 29 kb upstream and 41 kb downstream from the insertion site, respectively. No significant difference was observed in the relative transcript levels of LOC_Os06g24594 gene among mutant and WT. Interestingly, the uncharacterized DUF679 family gene (LOC_Os06g24490) expression was not detected in both mutant and WT that could be possibly due to its condition specific expression or non-functional gene. The *pap90* mutant was characterized in detail through morphological, physiological, molecular, and biochemical studies.

Morphological and yield characteristics of pap90 mutant

We observed that the homozygous *pap90* mutant showed clear unique differences from the WT. The mutant showed a significant reduction in flag leaf width (1.01 ± 0.05 cm-*pap90*; 1.51 ± 0.06 cm-WT) and area (39.5 ± 0.29 cm^2-*pap90*; 47.5 ± 0.51 cm^2-WT), but longer flag leaves (41.5 ± 1.67 cm-*pap90*; 32.1 ± 1.20 cm-WT) (Fig. 2A, B). The microscopic study of the flag leaf through SEM (Fig. 2C, D) revealed that the density of trichomes (Fig. 2CI) and silicon bodies (Fig. 2CII) were increased in *pap90* mutant as compared to WT. Also, the significant reduction by 24% in stomatal pore width of *pap90* mutant (6.14 ± 0.45 μm) was observed over WT (8.03 ± 0.35 μm) (Fig. 2DI, II). But the difference in stomatal pore length of WT (20.0 ± 0.88 μm) and *pap90* mutant (20.6 ± 0.47 μm) were statistically non-significant. Also, the yield associated traits like plant height, number of tillers, number of panicles, panicle length, number of grains per panicle, and grain yield per plant were analyzed. The significant variation was observed in the number of grains per panicle (122 ± 6.42- WT; 99 ± 6.52-*pap90*) and grain

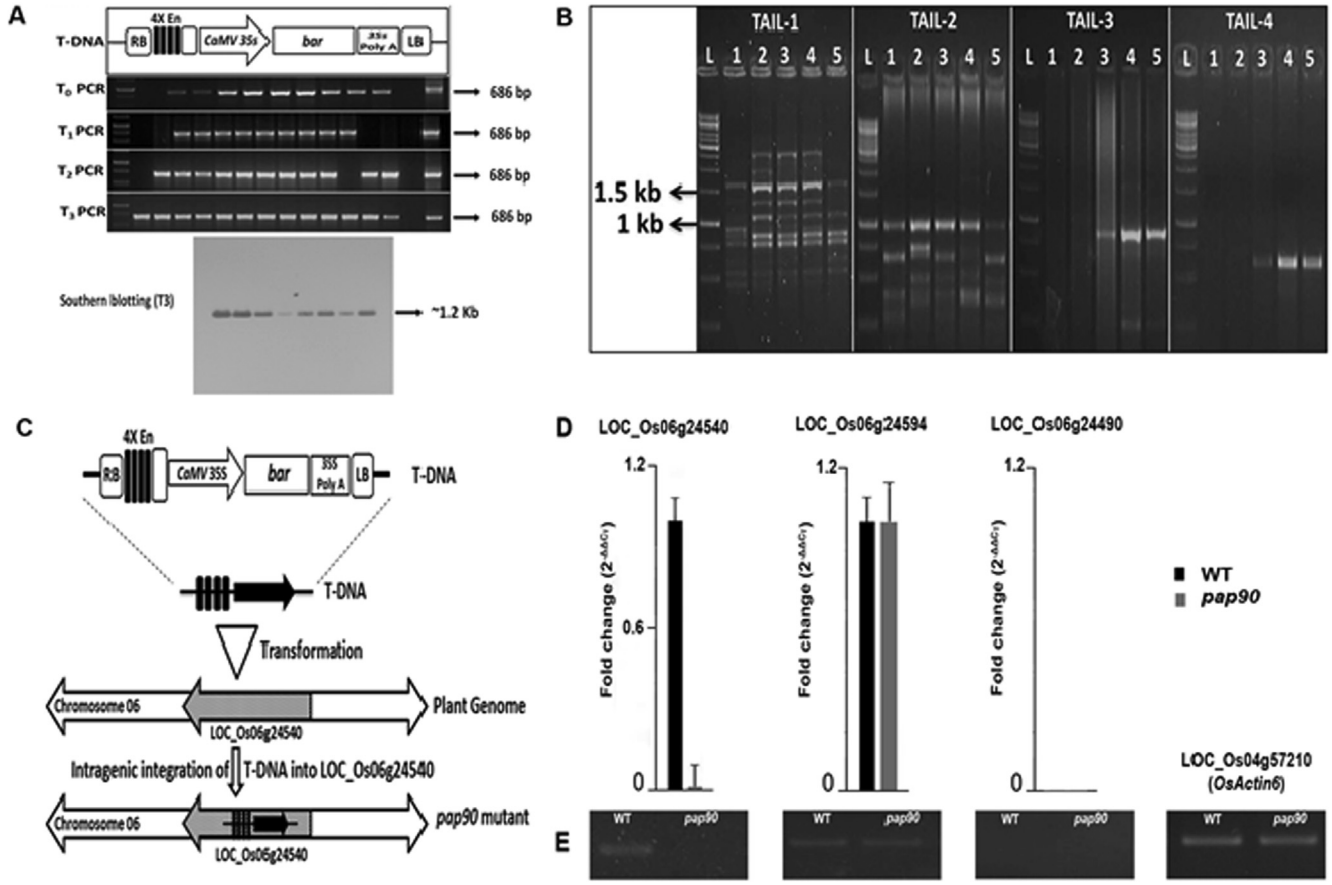

Fig. 1. Development and identification of *pap90* rice mutant (A) Linear map of En-Bar construct T-DNA region, molecular confirmation of *pap90* mutants at T_0, T_1, T_2, and T_3 generations through PCR and Southern blotting (T_3). (B) TAIL-PCR performed with five biological replicates of *pap90* mutant (n = 5), TAIL-1, TAIL-2, TAIL-3, and TAIL-4 are the nested PCRs. (C) Schematical representation of T-DNA insertion loci at intragenic region of LOC_Os06g24540 gene on chromosome 6. (D), (E) Relative expression analysis of LOC_Os06g24540, LOC_Os06g24594, and LOC_Os06g24490 genes in WT and *pap90* mutant by using qPCR and semi-quantitative PCR, respectively. Bars represent the mean ± SE of three biological replicates (n = 3). *OsActin* was used as internal control.

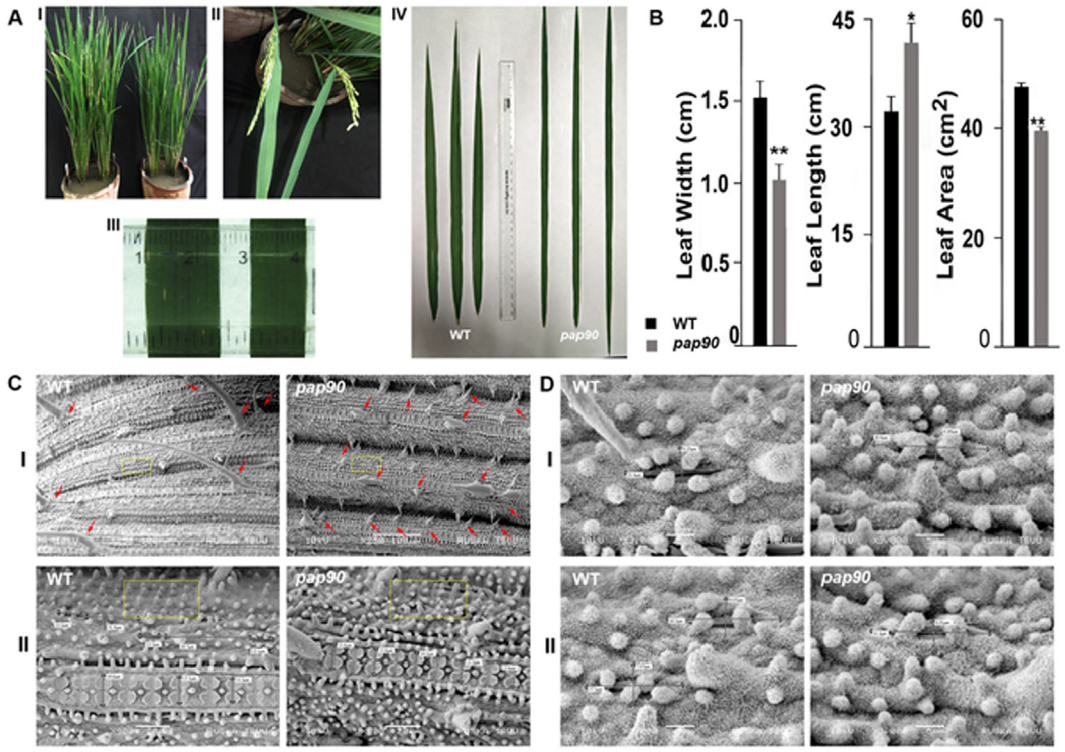

Fig. 2. Phenotype and morphological characteristics of *pap90* mutant (A) (I), (II), (III), and (IV) Phenotypic variations among *pap90* mutant and WT plants at flowering stage (~101 d old). (B) Graphical representation of phenotypic data viz. flag leaf width (cm), flag leaf length (cm), and flag leaf area (cm^2). Bars represent the mean ± SE of three biological replicates (n = 3). The mean values considered to be statistically significant at $P < 0.05$ (*statistically significant), and $P < 0.01$ (**very statistically significant) using a *t*-test and represented with asterisks. (C) SEM studies revealed the variation in (I) trichomes length and density in *pap90* and WT (indicating with red arrows), scale bars = 100 μm. (II) density of silica bodies on the leaf surface of *pap90* mutant and WT (indicating with a yellow box), scale bars = 20 μm. (D) (I), (II) Difference in stomatal pore width of *pap90* mutant and WT, scale bars = 5 μm.

yield (g) per plant (12.2 ± 1.32- WT; 8.6 ± 1.14-*pap90*) (Supplementary Figure S1E, F). The variations in other yield traits were statistically non-significant (Supplementary Figure S1A-D).

Introgression of functional OsPAP90 gene in pap90 mutant

The crosses were performed between the *pap90* and WT (*pap90* X WT) to introduce the functional *OsPAP90* gene into *pap90* mutant plants. Restoration of phenotype and the *OsPAP90* gene expression was analyzed in F1 recombinants (heterozygous condition). The resulted phenotype of ten recombinants (*pap90* X WT) was similar to WT (Fig. 3A, B). In *pap90* X WT plants, the flag leaf length (32.5 ± 0.32 cm) was equivalent to the WT (31.4 ± 0.41 c m) and lesser than *pap90* mutant (41.8 ± 1.09 cm). The leaf width of *pap90* X WT F1 plants (1.60 ± 0.04 cm) was equivalent to WT (1. 55 ± 0.06 cm) but higher than *pap90* mutant (1.20 ± 0.04 cm) (Fig. 3C, D). Further, the expression level of *OsPAP90* in the recombinant F1 plants was half of the expression recorded in WT (Fig. 3E). The results confirmed the *OsPAP90* disruption attributed to *pap90* phenotype.

Physiological characteristics of pap90 mutant

The differences in leaf morphology of mutant prompted us to probe if the photosynthetic parameters such as P_N, g_s, E, and C_i were affected (Fig. 4A-D). The P_N, g_s, E, and Ci were recorded as 13.37 ± 0.32 μmol CO_2 m^{-2} s^{-1}, 0.12 ± 0.01 mmol H_2O m^{-2} s^{-1}, 6.35 ± 0.28 mmol H_2O m^{-2} s^{-1}, and 165.65 ± 1.99 μmol CO_2 mol^{-1} in *pap90* mutant and 15.05 ± 0.07 μmol CO_2 m^{-2} s^{-1}, 0.25 ± 0.01 mmol H_2O m^{-2} s^{-1}, 8.99 ± 0.29 mmol H_2O m^{-2} s^{-1}, 228.78 ± 1.4 3 μmol CO_2 mol^{-1} in WT, respectively. The WUE (Fig. 4E) of mutant utilizes 2.11 ± 0.12 μmol of CO_2 per mmol H_2O transpired, while the WT utilizes 1.68 ± 0.06 μmols of CO_2 per mmol transpired H_2O. The iWUE (Fig. 4F) of mutant showed higher values as 108. 80 ± 4.10 μmols of CO_2 per mmol H_2O than the WT with 61.24 ± 2.91 μmols of CO_2 per mmol H_2O.

Despite the non-significant difference in total chl content (4.5 5 ± 0.42 mg g^{-1}FW-WT; 4.47 ± 0.34 mg g^{-1}FW-*pap90*) and relative water content (RWC) (85–95% in both WT and *pap90*) between mutant and WT (Supplementary Figure S2A, B), several photosynthetic parameters especially P_N were greatly affected in the mutant. The PSII efficiency (Fv/Fm) showed a reduction in the mutant (0.65 ± 0.02) compared to WT (0.72 ± 0.02) (Fig. 4G). Further, light response curve analysis revealed that ETR, qP, qN, and ϕPSII in mutant were negatively affected (Fig. 4H-K). These results together suggest that the PSII efficiency was significantly affected in mutants.

In-silico analysis of OsPAP90

The biological significance of *OsPAP90* gene in the *Oryza* sp. is still unknown. We identified a single copy *OsPAP90* gene in *Oryza* sp. genome while analyzing through BLASTP, TBLASTN (NCBI) and BLAST (RAP-DB). Further, PAP90 sequence analysis by using online tools like SMART, CDD, InterPro, Pfam, and HHpred revealed that the gene family was not yet classified. Phylogenetic analysis of PAP90 amino acid sequences indicated high variability among the homologous genes except for A0A096AV57 (*Zea mays*) and Sb01g037260.1 (*Sorghum bicolor*) (Supplementary Figure S3). Subsequently, alignment of PAP90 protein sequence over BLASTp [47]

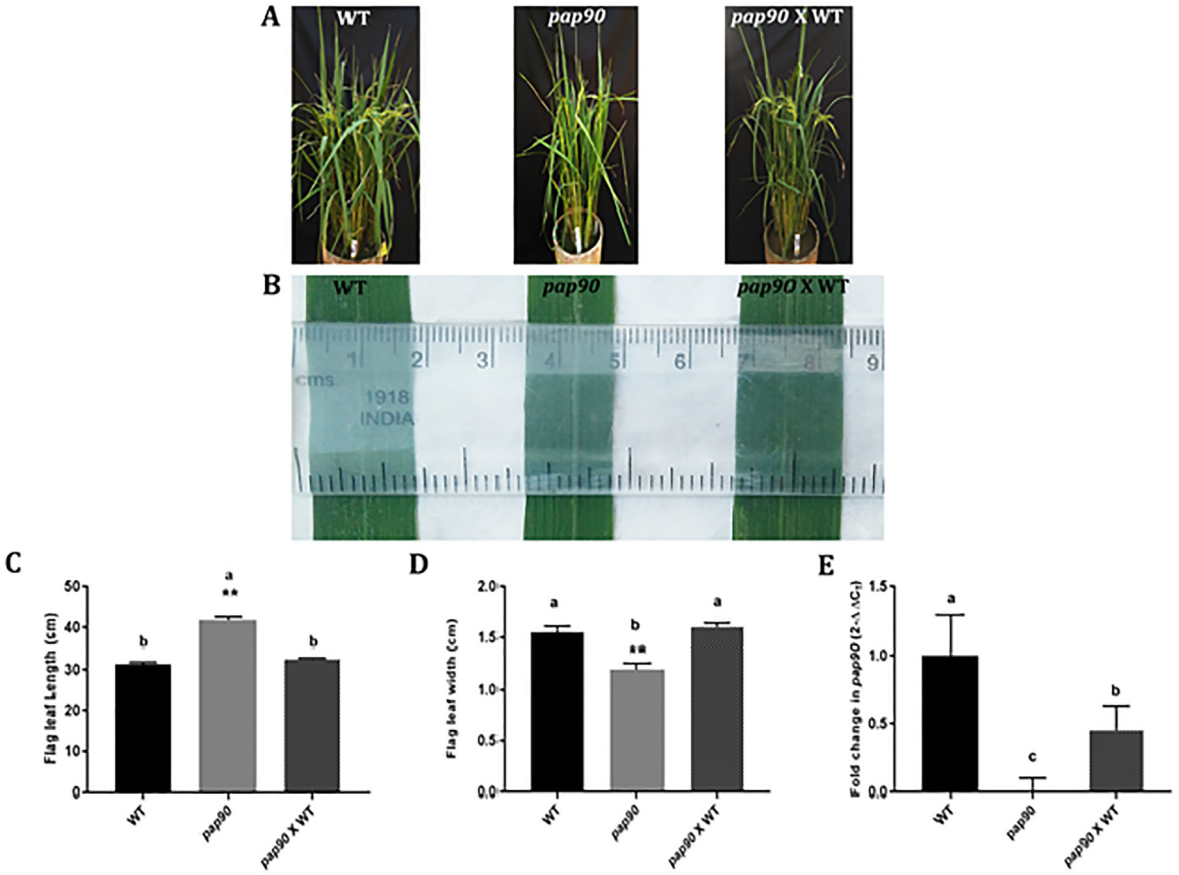

Fig. 3. Validation of *OsPAP90* gene through crossing (A), (B) Phenotypic variations in *pap90* mutant and F1 recombinants (*pap90* X WT) in comparison to WT. (C), (D) Graphical representation of variations in phenotypic data viz. flag leaf length (cm) and flag leaf width (cm), respectively, of *pap90* mutants and F1 recombinants when compared to WT. (E) Validation of *OsPAP90* gene in both parents (WT, *pap90* mutant) and F1 recombinants (*pap90* X WT) through qPCR. *OsActin* was used as an internal control. Bars represent the mean ± SE of three biological replicates (n = 3). The mean values considered to be statistically significant at $P < 0.05$ (*statistically significant), and $P < 0.01$ (**very statistically significant) using a *t*-test. Simultaneously, analysis of variance (ANOVA) was carried through Statistix Ver 8.1 and the significance of mean values determined by the least significant difference (LSD) test (alpha at 0.05).

showed most of the aligned proteins from dicots had similarities in the range from 37 to 42% only. Monocots like *Zea mays* and *Sorghum bicolor* showed 71–73% similarity (Supplementary Figure S3). In addition, protein–protein interaction network analysis of PAP90 through STRING predicted that the PAP90 directly interacted with D1 protein of PSII (Supplementary Figure S4A). In support, PAP90 was predicted to be a chloroplast transit peptide (cTP) as analyzed by Chlorop 1.1 prediction tool (Supplementary Figure S4B). These analyses predicted the close association among nucleus encoded PAP90 and chloroplast PSII-D1 protein.

Molecular and functional analysis of pap90 mutant

To further delineate the precise reasons for reduced PSII activity in *pap90* mutant, relative expression profiling of PSII associated genes was performed. The relative transcript levels of genes encoding PSII core subunits viz. *psb*A (D1), *psb*B (CP47), *psb*C (CP43), and *psb*D (D2) were statistically non-significant among mutant and WT (Supplementary Figure S5). Subsequently, 2DE revealed six differentially expressed proteins between mutants and WT (Fig. 5A) (Supplementary Table S5). The TDX_ORYSJ and COBL1_ORYSJ proteins could not be detected in *pap90* mutant. The other four protein spots viz., EXOS5_ORYSJ, RH38_ORYSJ, CSLF2_ORYSJ, and FTSH7_ORYSJ showed higher abundance in *pap90* mutant than WT. As per Mascot analysis, the protein score of RH38_ORYSJ and FTSH7_ORYSJ were significant.

The OsFtsH7, one amongst the high abundant proteins in *pap90*, is a nuclear-encoded FtsH gene family targeted to the chloroplast [17]. The expression analysis of genes encoding OsFtsH family (*OsFtsH1* to *OsFtsH9*, Supplementary Table S6) showed up-regulation by 2–3 folds in the mutant as compared to WT except for *OsFtsH6*, which could not be detected in both the *pap90* mutant as well as WT (Fig. 5B). The FtsH family proteins are involved in the degradation of the photodamaged D1 protein of PSII in *Arabidopsis* [48]. Mutation in *OsPAP90* affects the D1 protein stability, which in turn negatively regulates PSII efficiency, and leads to increased expression of OsFtsH family genes. Western blot analysis showed that the level of D1 protein of PSII was reduced in mutant. Densitometry-based quantification suggested that D1 protein was lowered by ~40% in the *pap90* mutant than WT (Fig. 5C). The results suggests that the FtsH proteins mediated degradation of D1 protein might be responsible for the reduction in D1 protein levels.

In continuation, the association dynamics of protein complexes in thylakoid membrane of chloroplast were studied through BN-SDS PAGE (Fig. 6A). Based on previous reports [13,30], bands were considered as follows: I: PSII supercomplexes; II: monomeric PSI and LHCII; III: PSI core; IV: monomeric PSII; V: F1 ATPase; VI: cp43 minus PSII; VII: trimeric LHCII; VIII: dimeric LHCII and IX: monomeric LHCII. PSII supercomplex was absent or hardly detected in mutant (Fig. 6AI). We also observed a reduction in band intensities of other mutant complexes (II, IV, and VI) through non-gradient and gradient BN-SDS PAGE gels (Fig. 6AI, II, respectively). The reduced D1 levels, negatively regulated the association

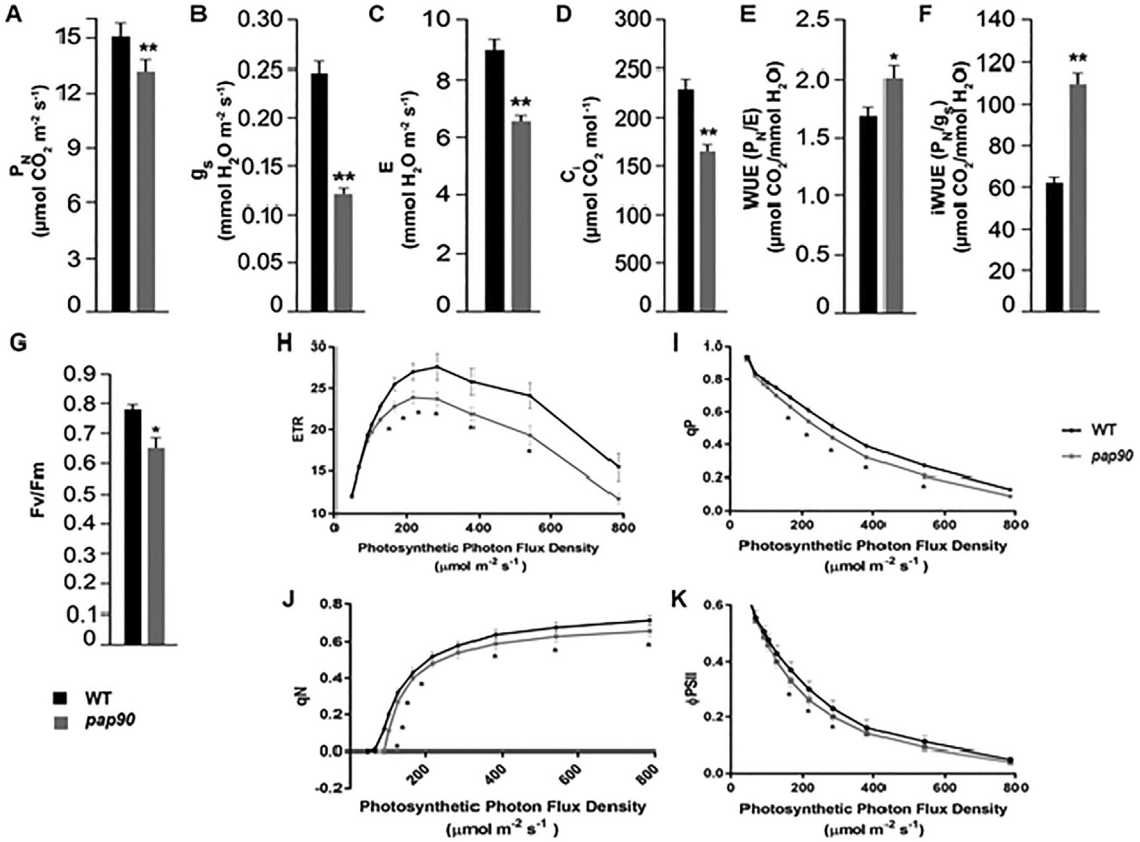

Fig. 4. Physiological characteristics of *pap90* mutant, Variations in the physiological parameters of *pap90* mutant when compared with WT viz., (A) Net photosynthesis rate (P_N). (B) Stomata conductance (g_s). (C) Transpiration rate (E). (D) Intercellular CO_2 (Ci). (E) Water use efficiency (WUE: P_N/E). (F) intrinsic water use efficiency (iWUE: P_N/g_s). (G) Variation in the chlorophyll fluorescence parameters Fv (Fm-Fo: variable fluorescence) and Fm (maximum fluorescence) represented as maximum quantum efficiency of PSII (Fv/Fm). Bars represent the mean ± SE of three biological replicates (n = 3). Significant reduction in (H) ETR: Electron transport rate. (I) qP: coefficient of photochemical quenching. (J) qN: coefficient of non-photochemical quenching. (K) ϕPSII: effective PSII quantum yield in the mutant when compared with WT. Points represent the mean ± SE of three biological replicates (n = 3). The mean values considered to be statistically significant at P < 0.05 (*statistically significant), and P < 0.01 (**very statistically significant) using a *t*-test.

dynamics of PSII and associated membrane complexes that could be responsible for the decreased PSII efficiency.

To provide further evidence, Y2H assays were performed to show the interaction between PAP90 and D1 proteins (Fig. 6B). The recombinant BD and AD vectors were transformed into Y2HGold and Y-187 strains, respectively. The ability of mated recombinant yeast growth on SD drop out medium was considered as a positive indication for the interaction between the proteins. The growth of mated yeast was observed only in combinations of BD-PAP90/AD-D1 and BD-D1/AD-PAP90 on TDO and QDO medium along with positive control (BD-p53/AD-T). At the same time growth was not detected in other combinations along with negative control (BD-Lamin/AD-T). Therefore, we confirmed that PAP90 had direct interaction with D1 protein [13] (Fig. 6B). In addition, TEM (Fig. 6C) studies of *pap90* mutant and WT leaves provided valuable information about variations in the ultrastructure of chloroplast. Particularly, the size/area of the chloroplast was shrunken significantly by 29% in *pap90* mutant (1.07 ± 0.009) as compared to WT (1.50 ± 0.053). Taken together, this evidences suggest that the PAP90 interacts with D1 protein and regulates its stability, thereby promotes the subsequent assembly of PSII and associated membrane complexes.

Association of OsPAP90 mutation with abiotic stress response

2DE results showed the over-expression of RH38_ORYSJ in the mutant that plays an important role in the positive regulation of CBF/DREB transcription factors involved in abiotic stress response (Fig. 5A) (Supplementary Table S5). The *OsPAP90* gene expression profile was investigated in WT under different stress conditions like NaCl, PEG, ABA, and dark treatments (24 h). Results showed up-regulation of *OsPAP90* gene by 1.5 and 1.6 fold under NaCl and dark stresses, respectively, however, it was down-regulated under PEG and ABA treatments by 2.3 and 1.6-folds, respectively (Fig. 7A). Further, we studied the relative expression level of various stress-responsive genes [22] in both the mutant and WT. Among them, *DREB2A*, *NAC6,* and *Zip23* genes were up-regulated in the mutant by 1.3, 2.9, and 1.4-folds, respectively over WT (Fig. 7B). Also, the accumulation of TSS and starch was more in the flag leaves of mutant (125.6 ± 0.63 mg g^{-1}FW; 100.5 ± 0.77 m g g^{-1}FW, respectively) than WT (84.6 ± 1.28 mg g^{-1}FW; 61.8 ± 0.6 5 mg g^{-1}FW, respectively) (Fig. 7C). The resulted variations in mutant corroborated the *OsPAP90* gene association with various abiotic stresses either directly or indirectly.

Further, we examined the accumulation of ROS species such as O_2^- and H_2O_2 in the flag leaf using NBT and DAB staining, respectively. Interestingly, both O_2^- and H_2O_2 concentrations were significantly higher in the mutant than WT (Fig. 8A, B). The spectrophotometric quantification revealed that the H_2O_2 content was increased by 11% in *pap90* mutant (3.41 ± 0.029 µmol g^{-1}FW) than WT (3.08 ± 0.03 µmol g^{-1}FW) (Supplementary Figure S6). The MDA levels were increased by 18% in the *pap90* mutant (8.32 ± 0.0 1) over WT (7.03 ± 0.03) (Fig. 8C). Furthermore, the activity of ROS scavenging enzymes such as SOD, CAT, and APX was increased by

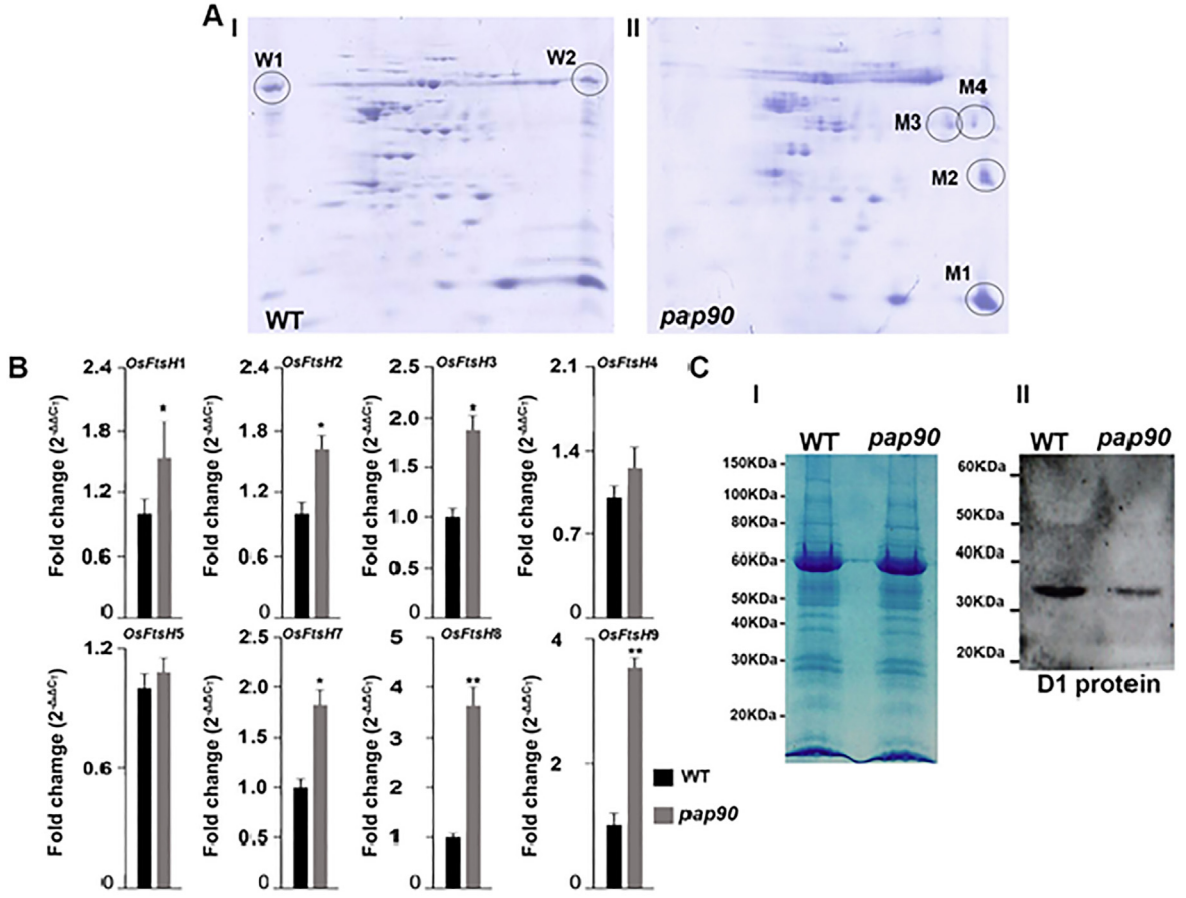

Fig. 5. Molecular analysis of *pap90* mutant (A) Proteomic analysis of WT and mutant through 2DE (2- dimensional gel electrophoresis), W1 and W2: overexpressed in WT than *pap90* mutant, M1-M4: overexpressed in *pap90* mutant than WT. (B) Relative expression analysis of OsFtsH family genes in WT and mutant. *OsActin* was used as an internal control. Bars represent the mean ± SE of three biological replicates (n = 3). The mean values considered to be statistically significant at $P < 0.05$ (*statistically significant), and $P < 0.01$ (**very statistically significant) using a *t*-test. (C) (I) quantitative analysis of protein from WT and *pap90* mutant through SDS-PAGE. (II) The quantitative detection of D1 protein in mutant over WT studied through Western blotting, probed with Anti D1.

13%, 11% and 17%, respectively in the mutant (8.39 ± 0.06, 23.9 ± 0.26 and 35.7 ± 1.08) as compared to WT (7.40 ± 0.23, 21.6 ± 0.72 and 30.4 ± 0.31) (Fig. 8D-F). Thus, the data suggested that PAP90 dysfunction induces the stress-associated genes, and accumulation of ROS, the signaling molecules in stress response pathways.

Phenotyping of pap90 mutant against abiotic stresses

The correlation between resulted changes in *pap90* mutant and its behavior was studied under various abiotic stresses. In WLS stress, ten plants from stable T_4 homozygous lines of mutant and WT were screened against WLS, and another set of plants were maintained as control. After the commencement of water stress, WT plants started wilting from 10 to 12 d onwards, while the mutant did not show any stress symptoms until three weeks (18–21 d) (Fig. 9A). The observed phenotype suggested that *pap90* showed better adaptation for WLS than WT. Photosynthetic parameters such as P_N, g_s, E, and Ci were analyzed 10 d after the commencement of WLS. While comparing the plants under stress with unstress, P_N, g_s, and E were reduced by 67%, 73%, and 63% in WT stress plants, and 51%, 64%, and 56% in mutant stress plants, respectively. In contrast, Ci was increased by 13% and 6% in WT and mutant, respectively, under stress. The WUE was reduced by 11% in WT but increased by 13% in the mutant under stress. The iWUE increased in both WT and mutant by 21% and 45%, respectively, under stress (Fig. 9B). Significant enhancement of the proline content in the mutant (42.6 ± 2.78 μg g^{-1}FW) was observed when compared with WT (14.4 ± 1.16 μg g^{-1}FW) (Fig. 9C) under stress condition. These observations suggested better performance of mutant than WT under WLS.

In continuation to previous experiment of *OsPAP90* gene association with abiotic stress, both *pap90* and WT plants were screened against dark stress. The conspicuous phenotypic differences were detected after 15 d of dark stress between the mutant and WT. Particularly, the chlorosis rate was rapid in mutant (Supplementary Figure S7A). The relative expression studies of photosynthesis associated genes [46] were performed at 0, 24, 48, and 72 h of dark stress (Supplementary Figure S7B). At 0 h, the expression of genes was down-regulated significantly in the mutant. But from 24 to 72 h, *psaA* gene expression was slightly upregulated at 24 and 48 h of dark stress but down-regulated at 72 h. While, expression of other genes such as *rbcL, rbcS*, *Cab1*, *Cab2,* and *Cao1* was gradually reduced in both mutant and WT but reduction was comparatively more in *pap90* mutant. In addition, we identified the light-responsive *cis*-elements in upstream sequences of *OsPAP90* such as AE (1 AGAAACAA), ACE (2 ACGTGGA); G-Box (5 CACGTC); GT-1 (1 ATGGTGGTTGG); Sp1 (8 CC(G/A)CC(C/G)GGCGG). These results indicate that the *pap90* mutant was susceptible to dark stress over WT. From these studies, we conclude that *OsPAP90* is a single dominant gene that involved in D1 protein stability and subsequently, promotes the assembly and function of PSII and associated complexes.

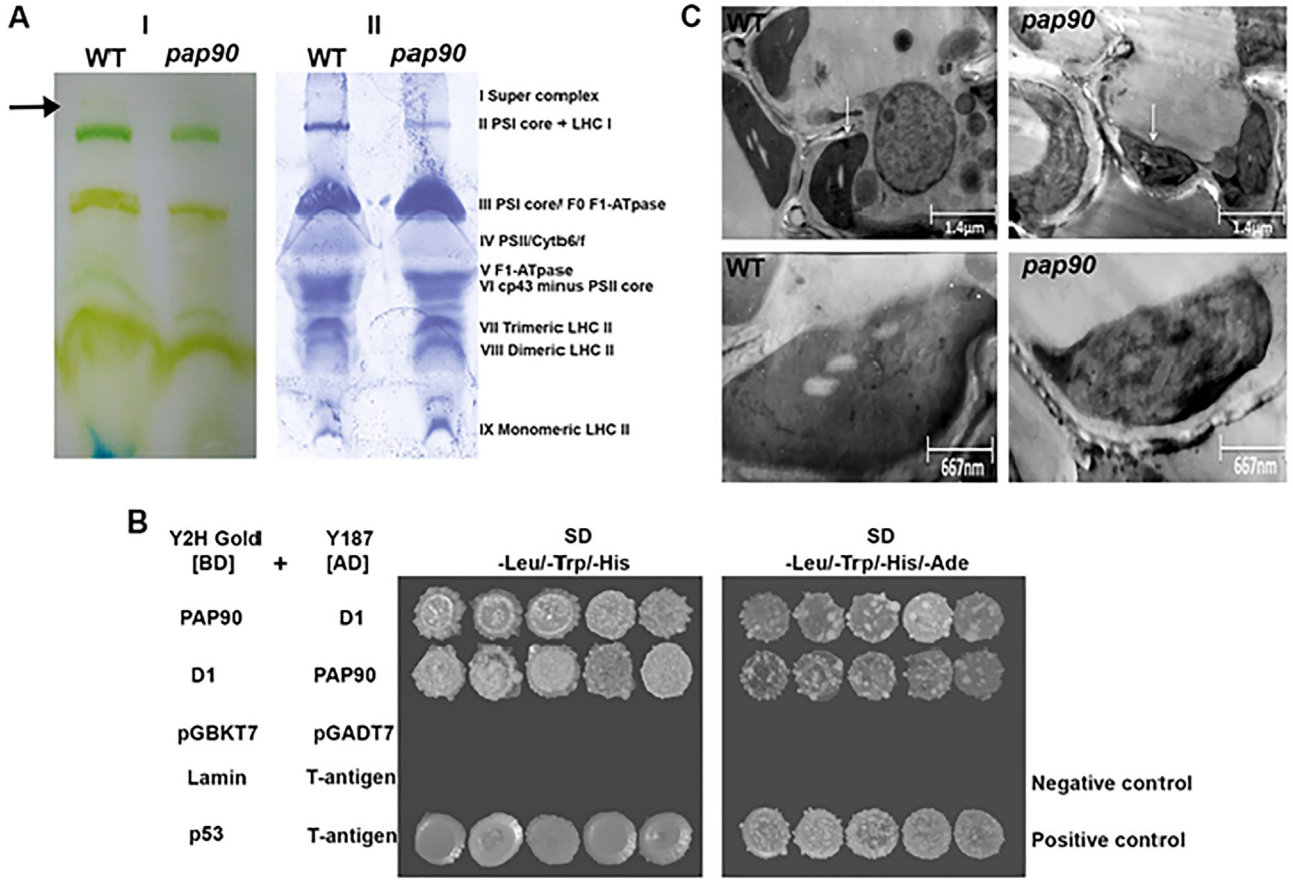

Fig. 6. Functional analysis of *OsPAP90* gene (A) Solubilized thylakoid protein complexes (I: 75 µg; II: 125 µg chlorophyll, respectively) separated on (I) non-gradient and (II) gradient gels by BN-SDS PAGE (black arrow indicating the PSII supercomplex), respectively. (B) PAP90 protein interacts with D1 in yeast two-hybrid assay. Full-length CDs of *OsPAP90* (PAP90) was fused with the GAL4 binding domain (BD) and *psbA* (D1) was fused with the GAL4 activation domain (AD) and vice versa and transformed into Y2HGold and Y187 strains, respectively. Yeast transformants were spotted on synthetically defined (SD) drop out medium (TDO:-Leu/-Trp/-His and QDO:-Leu/-Trp/-His/-Ade). BD-p53/AD-T and BD-Lam/AD-T are positive and negative controls, respectively. (C) Structure of chloroplast observed in *pap90* mutant and WT through TEM studies (indicating with white arrow).

Discussion

Photosystem II is a multi-subunit protein complex of several uncharacterized nuclear-encoded proteins that play a significant role in the formation of functional PSII complex. Precise roles and mechanistic aspects of these uncharacterized proteins in the formation of functional PSII complex largely remain unknown [7]. This study describes one such nuclear-encoded protein that affects D1 protein stability and PSII efficiency. The loss-of-function mutant was obtained by T-DNA integral disruption of *OsPAP90* gene in *Oryza sativa* L., subsp *indica*. Based on the site of synthesis and localization, the uncharacterized protein was named as PSII auxiliary protein with molecular weight ~90 kDa (PAP90). The protein-encoding gene and loss-of-function mutant were represented as *OsPAP90* and *pap90*, respectively. The characteristics of the mutant were investigated using various approaches to present evidence that the *OsPAP90* gene is a novel nuclear-encoded gene associated with D1 protein stability and subsequently, involved in the PSII association dynamics.

'Activation-tagging' mutagenesis approach based on CaMV 35S 4X enhancer was used to activate the expression of nearby genes [49]. The enhancer tagged rice native genes led to the gain-of-function mutants with phenotypic variations [50]. Another reason for the phenotypic variations is loss-of-function due to the disruption of the native functional genes. In this case, the phenotypic changes in the mutant were attributed to loss-of-function due to the disruption of the single dominant gene *OsPAP90*. The PAP90 is a nuclear-encoded protein and predicted to be a cTP. A homologous protein, HCF243 from *Arabidopsis thaliana* has been shown as a chloroplast-localized protein that affects PSII assembly [13]. Unlike *hcf243* mutant of *Arabidopsis*, the *pap90* mutant of rice did not show any dwarf phenotype, but displayed variations viz. reduction in leaf area, leaf width, stomatal pore width, chloroplast ultrastructure, number of grains per panicle, grain yield per plant and increase in flag leaf length, trichomes, and silicon body density on the leaf surface. Concomitant with these phenotypic and morphological differences, photosynthesis parameters such as P_N, g_s, E and C_i were significantly reduced in mutant without any notable differences in chl content as well as RWC. The internal factors affecting the process of photosynthesis are water content of leaf [51], chl, and the enzymatic or regulatory factors [52]. Therefore, the variation in photosynthetic parameters in mutant was possibly due to dysfunction of a regulatory factor, PAP90. Chl florescence study is an effective tool for analyzing the functional activity of PSII by measuring quantum efficiencies in dark and light (Fv/Fm) [53]. Fv/Fm values positively correlate with PSII activity [54]. The dysfunction of PAP90 caused a significant reduction of Fv/Fm, ETR, qP, and qN at high PPFD in *pap90* mutant indicating the reduction in PSII activity and efficiency. Among these, qN is considered an important regulatory factor that protects the reaction center of PSII against photoinhibition [55]. Reduction of qN together with qP in the *pap90* mutant plants rendered as photoinhibition sensitive.

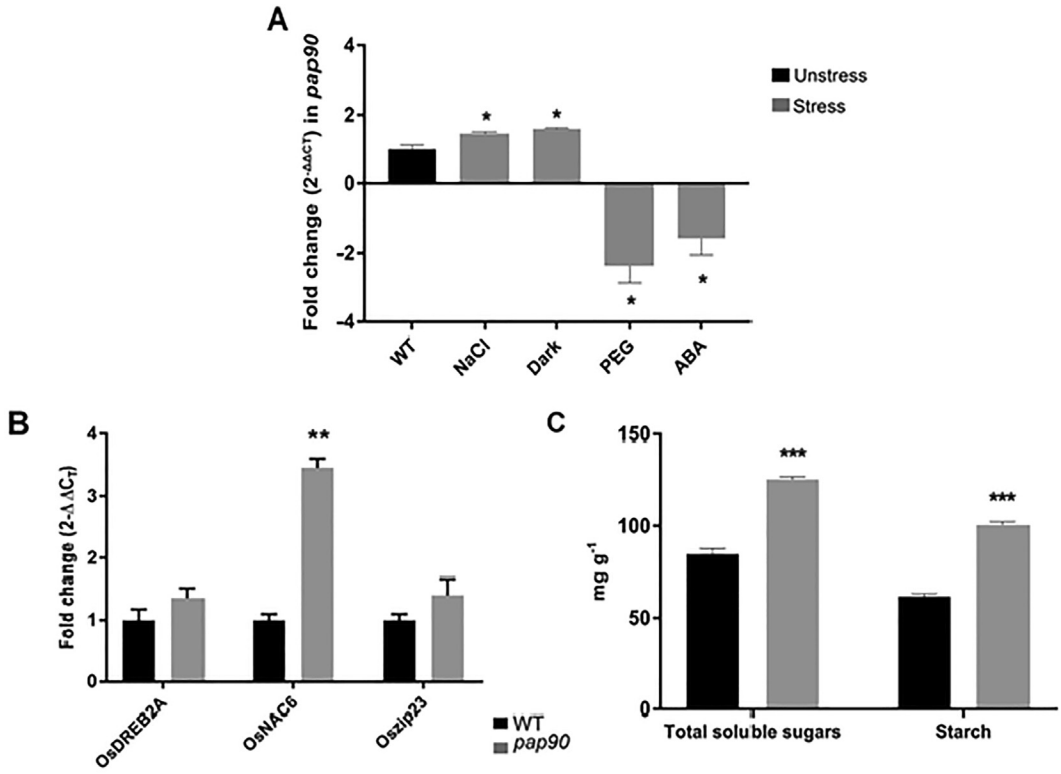

Fig. 7. Abiotic stress response adaptations in *pap90* mutant (A) Relative expression analysis of *OsPAP90* gene in WT under various abiotic stresses after 24 h treatment when compared with unstress condition viz. NaCl, Dark, PEG, and ABA. (B) Relative expression analysis of various transcription factors viz. *OsDREB2A*; *OsNAC6*; *OsZip23* in mutant compared with WT. *OsActin* was used as an internal control. (C) Determination of total soluble sugars (TSS) and starch content in flag leaves of both WT and *pap90* mutant. Bars represent the mean ± SE of three biological replicates (n = 3). The mean values considered to be statistically significant at P < 0.05 (*statistically significant), P < 0.01 (**very statistically significant), and P < 0.001 (***extremely statistically significant) using *t*-test.

Further, the OsFtsH7 protein, belonging to the FtsH family accumulated in *pap90* mutant. The FtsH family proteins are mainly chloroplast localized proteins involved in the degradation of damaged D1 protein of PSII [48]. Even though relative transcript levels of major subunits of PSII remain comparable, the D1 protein levels have been significantly reduced in *pap90* mutant, which might be associated with up-regulation of OsFtsH family genes. Rapid degradation of D1 protein might be responsible for the inadequate accumulation of the thylakoid membrane complexes. The physical interaction of PAP90 with D1 protein suggests that PAP90 may protect and stabilize D1 protein. The structure of chloroplast influences the photosynthesis rate as well plant growth and development [56]. TEM studies showed that the structure of chloroplast was shrunken in *pap90* mutant. Therefore, our data suggests that in absence of PAP90, D1 protein was unstable that subsequently leads to reduction in PSII efficiency.

The reduced D1 protein levels may disturb the efficiency of photosynthetic ETR, carbon reduction cycle, and PSII in *pap90* mutant that induces the production of ROS which inhibits the PSII damage repair system by preventing the D1 protein synthesis [57,58,59]. Increased activity of antioxidant enzymes such as SOD, CAT, and APX provided further evidence of enhanced ROS due to *OsPAP90* gene disruption. Previous studies reported that ROS accumulation plays a key role in signal transduction to activate the stress response pathways [60]. Thus, we presumed that the stress-responsive pathways in *pap90* mutant might be activated.

Notably, RH38_ORYSJ protein was induced in a *pap90* mutant. In *Arabidopsis*, this protein plays an essential role in development and stress response [61]. Also, the RH38_ORYSJ is a positive regulator of transcription factors like CBF/DREB, which play a key role in abiotic stress tolerance like cold, drought, and salt through ABA-dependent/ independent pathways [62]. Induced expression of transcription factors such as *OsDREB2A*, *OsNAC6,* and *OsbZip23* was noticed in *pap90*, which are key players for various stress-tolerant pathways viz. drought, cold and salt stresses [63]. Incidentally, native *OsPAP90* gene expression in WT was positively regulated under salt and dark stresses and negatively regulated under PEG and ABA stresses. Therefore, we anticipated that the *pap90* mutant might respond positively to PEG and ABA, and negatively for salt and dark stress treatments.

Further investigations supported our hypothesis as *pap90* mutant showed better adaptability than WT under WLS. In support, TSS and starch were highly pre-accumulated in the mutant. The sugars play a major role in plant stress tolerance [64]. The variability in length, density, and distribution of trichomes plays a significant role in stress tolerance [65]. Also, increased silicon bodies reduce the cuticular transpiration and improve the WUE [66]. Reduction in stomata pore width lowers the g_s that improve WUE [67]. Further, the accumulation of an proline in mutant augment its stress tolerance ability [25]. Overall, increased trichomes and silicon body density on leaf surfaces, pre-accumulation of sugars, and stress-induced proline accumulation in *pap90* mutant might contribute to the better adaptability of *pap90* under WLS. In mutants, sometimes loss of one function may lead to the gain of another function. The loss-of-function of rice membrane protein SLAC7 led to a reduction in chloroplast stability but induced photoprotection in rice [68]. The resulted changes in *pap90* mutant increased the dark stress sensitivity. The continuous dark stress induces the leaf senescence that causes chl and protein degradation [69]. The leaf senescence mediated chl degradation was rapid in *pap90* mutant over WT that led to chlorosis. The leaf senescence is negatively associated with enhanced expression of PSII related

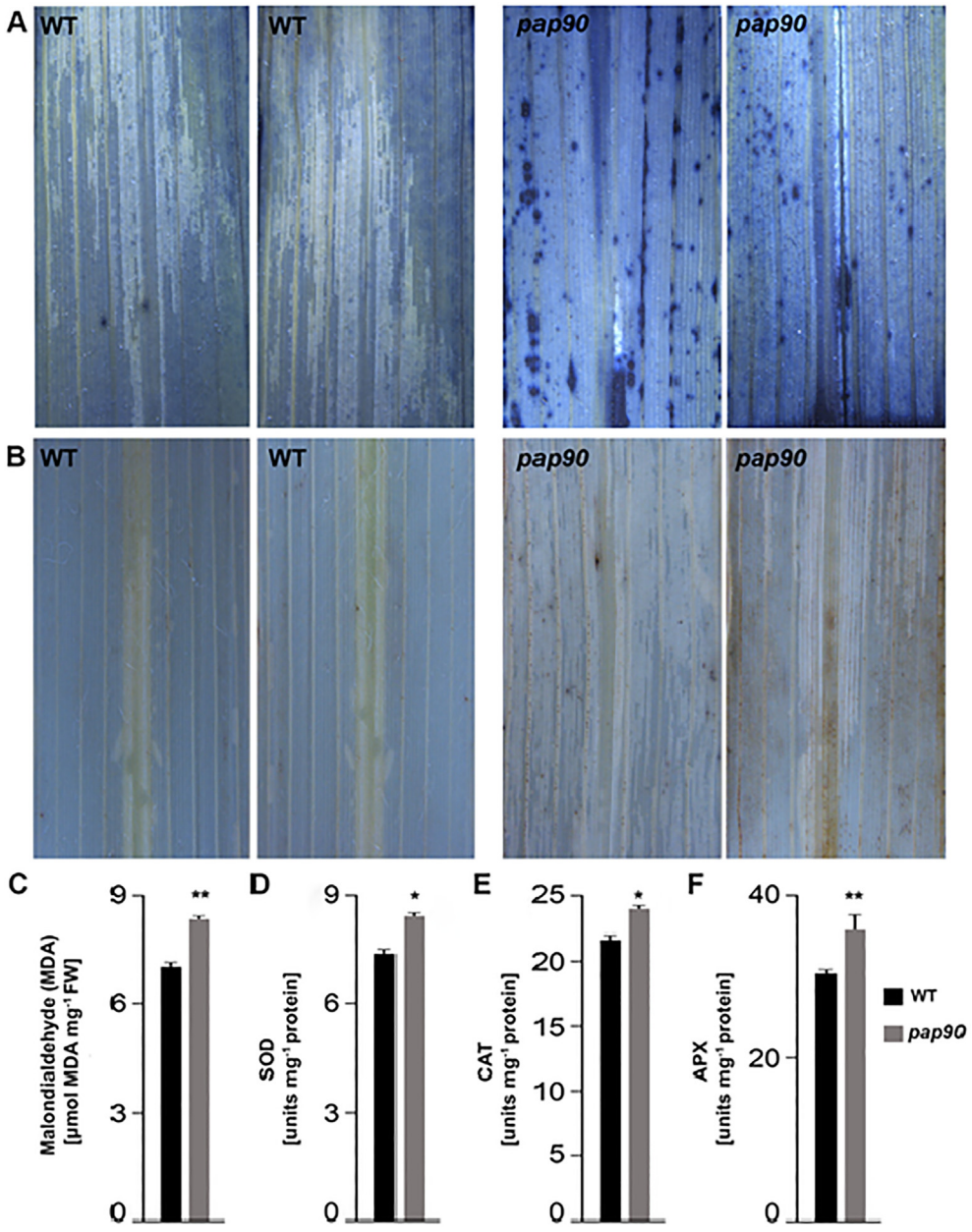

Fig. 8. Biochemical adaptations in *pap90* mutant (A) Detection of superoxide radicals (O_2–) through NBT staining (blue color spots indicating the superoxide radicals) in WT and *pap90* mutant. (B) Detection of hydrogen peroxide (H_2O_2) through DAB staining (brown color spots indicating the hydrogen peroxide) in WT and *pap90* mutant. (C) Estimation of lipid peroxidation through malonaldehyde content in WT and *pap90* mutant. Analysis of antioxidant enzymes activity in WT and mutant. (D) Superoxide dismutase (SOD). (E) Catalase (CAT). (F) Ascorbate peroxidase (APX). Bars represent the mean ± SE of three biological replicates (n = 3). The mean values considered to be statistically significant at P < 0.05 (*statistically significant), P < 0.01 (**very statistically significant), and P < 0.001 (***extremely statistically significant) using *t*-test.

genes and stability of photosynthetic complexes [70]. We also noticed significant down-regulation of chl and photosynthesis associated genes under dark stress. In response to stresses, plants can reprogram their growth by various unknown mechanisms [71]. In this study, we hypothesized the plant adaptive mechanisms in mutant against loss-of-function of *OsPAP90* gene.

Through this study, we report that the *OsPAP90* is a single dominant gene of rice. Interestingly, *OsPAP90* gene presence is restricted to flowering plants, especially, high homology with monocots. The *OsPAP90* gene encodes a protein that regulates the D1 protein stability that subsequently promotes PSII and associate complexes assembly and efficiency. The disruption of *OsPAP90* caused several morphological, physiological, molecular, and biochemical changes which resulted in decreased photosynthesis and grain yield but improved adaptability for water-limited stress. A recent study substantiated our phenotypic observations of the *pap90* mutant [72]. D1 protein strongly influences photosynthetic efficiency and yield of rice [72]. Though many factors involved in the ancient process of photosynthesis have been identified and characterized in model plants like *Arabidopsis*, the discovery of novel photosynthesis associated proteins in food crops like rice will open new avenues for enhancing the crop productivity and stress tolerance.

Compliance with ethics requirements

This article does not contain any studies with human or animal subjects

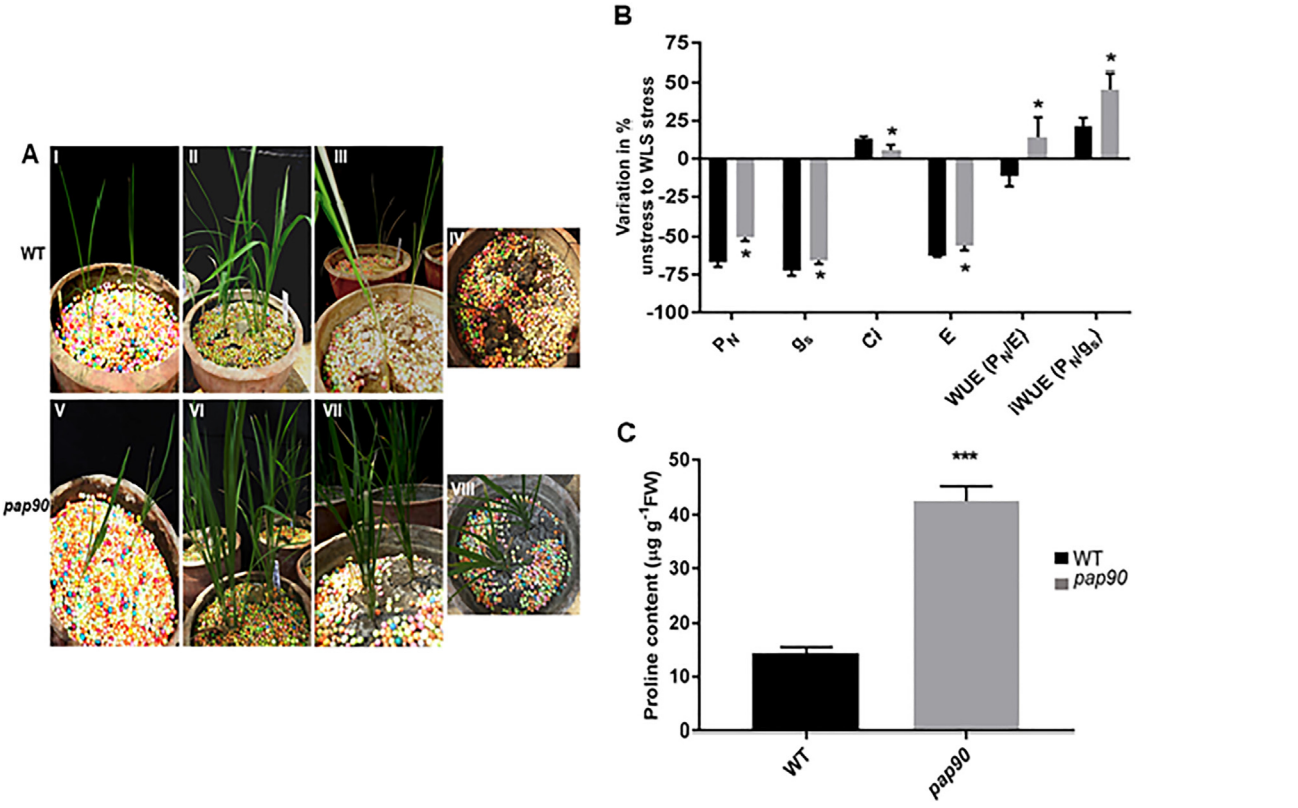

Fig. 9. Phenotyping and physiological adaptations of *pap90* mutant under WLS (A) Water limited stress experiment. (I) 15 d old WT plantlets transferred to earthen pots. (II) six-week-old WT plants under well-watered condition. (III), (IV) six-week-old WT plants under three weeks water stress. (V) 15 d old *pap90* mutant plantlets transferred to earthen pots. (VI) six-week mutant plants under well-watered condition. (VII), (VIII) six-week-old mutant plants under three weeks of water stress. (B) Graphical representation of variations in photosynthetic parameters like P_N, g_s, E, Ci, WUE, and iWUE from control to stress condition of both WT and mutant individually. (C) Determination of proline content in both WT and *pap90* mutant under WLS stress. Bars represent the mean ± SE of three biological replicates (n = 3). The mean values considered to be statistically significant at P < 0.05 (*statistically significant), P < 0.01 (**very statistically significant), and P < 0.001 (***extremely statistically significant) using *t*-test.

Declaration of Competing Interest

The authors declare that they have no known competing financial interests or personal relationships that could have appeared to influence the work reported in this paper.

Acknowledgments

Authors are thankful to Prof. P. B. Kirti, University of Hyderabad, India for providing the binary vector. Thankfully acknowledge the financial support from the Department of Biotechnology (DBT), India, funded through network project with sanction File No. BT/PR-13105/AGR/02/684/2009.

Author contribution statement

Transformation, molecular characterization, and In-silico analysis: MRR, SVR, PM, and PNB; Crossing, Screening, Physiological and Biochemical studies: MRR, PY, TVK, and DS; Conception, designing and overall guiding of the execution of the experiments: SMB, SKM, RMS; Data analysis and drafting of the manuscript together with MRR., SKM., and SMB.

Appendix A. Supplementary material

Supplementary data to this article can be found online at https://doi.org/10.1016/j.jare.2020.11.008.

References

[1] Tsuchida-Mayama T, Nakamura H, Hakata M, Ichikawa H. Rice transgenic resources with gain-of-function phenotypes. Breed Sci 2010;60:493–501. doi: https://doi.org/10.1270/jsbbs.60.493.
[2] Hsing YI, Chern CG, Fan MJ, Lu PC, Chen KT, Lo SF, et al. A rice gene activation/knockout mutant resource for high throughput functional genomics. Plant Mol Biol 2007;63:351–64. doi: https://doi.org/10.1007/s11103-006-9093-z.
[3] Ayliffe MA, Pryor AJ. Transposon-based activation tagging in cereals. Funct Plant Biol 2009;36:915–21. doi: https://doi.org/10.1071/FP09130.
[4] Sinclair TR, Purcell LC, Sneller CH. Crop transformation and the challenge to increase yield potential. Trends Plant Sci 2004;9:70–5. doi: https://doi.org/10.1016/j.tplants.2003.12.008.
[5] Nelson N, Ben-Shem A. The complex architecture of oxygenic photosynthesis. Nat Rev Mol Cell Biol 2004;5:971–82. doi: https://doi.org/10.1038/nrm1525.
[6] Rokka A, Suorsa M, Saleem A, Battchikova N, Aro EM. Synthesis and assembly of thylakoid protein complexes: Multiple assembly steps of photosystem II. Biochem J 2005;388:159–66. doi: https://doi.org/10.1042/BJ20042098.
[7] Rochaix JD. Assembly of the photosynthetic apparatus. Plant Physiol 2011;155:1493–500. doi: https://doi.org/10.1104/pp.110.169839.
[8] Dekker JP, Boekema EJ. Supramolecular organization of thylakoid membrane proteins in green plants. Biochim Biophys Acta - Bioenerg 2005;1706:12–39. doi: https://doi.org/10.1016/j.bbabio.2004.09.009.
[9] Barber J. Photosystem II: the water splitting enzyme of photosynthesis and the origin of oxygen in our atmosphere. Q Rev Biophys 2016;49. doi: https://doi.org/10.1017/s0033583516000093.
[10] Moore M, Harrison MS, Peterson EC, Henry R. Chloroplast Oxa1p homolog albino3 is required for post-translational integration of the light harvesting chlorophyll-binding protein into thylakoid membranes. J Biol Chem 2000;275:1529–32. doi: https://doi.org/10.1074/jbc.275.3.1529.
[11] Plücken H, Müller B, Grohmann D, Westhoff P, Eichacker LA. The HCF136 protein is essential for assembly of the photosystem II reaction center in Arabidopsis thaliana. FEBS Lett 2002;532:85–90. doi: https://doi.org/10.1016/S0014-5793(02)03634-7.

[12] Meurer J, Plücken H, Kowallik KV, Westhoff P. A nuclear-encoded protein of prokaryotic origin is essential for the stability of photosystem II in Arabidopsis thaliana. EMBO J 1998;17:5286–97. doi: https://doi.org/10.1093/emboj/17.18.5286.
[13] Zhang D, Zhou G, Liu B, Kong Y, Chen N, Qiu Q, et al. HCF243 encodes a chloroplast-localized protein involved in the D1 protein stability of the Arabidopsis Photosystem II complex. Plant Physiol 2011;157:608–19. doi: https://doi.org/10.1104/pp.111.183301.
[14] Foyer CH, Leiandais M, Kunert KJ. Special review Photooxidative stress in plants. Physiol Plant 1994;92:696–717.
[15] Nishiyama Y, Murata N. Revised scheme for the mechanism of photoinhibition and its application to enhance the abiotic stress tolerance of the photosynthetic machinery. Appl Microbiol Biotechnol 2014;98:8777–96. doi: https://doi.org/10.1007/s00253-014-6020-0.
[16] Kusaba M, Ito H, Morita R, Iida S, Sato Y, Fujimoto M, et al. Rice non-yellow coloring1 is involved in light-harvesting complex II and grana degradation during leaf senescence. Plant Cell 2007;19:1362–75. doi: https://doi.org/10.1105/tpc.106.042911.
[17] Wang F, Liu J, Chen M, Zhou L, Li Z, Zhao Q, et al. Involvement of abscisic acid in PSII photodamage and D1 protein turnover for light-induced premature senescence of rice flag leaves. PLoS ONE 2016;11:1–25. doi: https://doi.org/10.1371/journal.pone.0161203.
[18] Yu F, Park S, Rodermel SR. Functional redundancy of AtFtsH metalloproteases in thylakoid membrane complexes. Plant Physiol 2005;138:1957–66. doi: https://doi.org/10.1104/pp.105.061234.
[19] Adam Z, Adamska I, Nakabayashi K, Ostersetzer O, Haussuhl K, Manuell A, et al. Chloroplast and mitochondrial proteases in Arabidopsis. A proposed nomenclature. Plant Physiol 2001;125:1912–8. doi: https://doi.org/10.1104/pp.125.4.1912.
[20] Benfey PN, Chua N. CaMV 35S enhancer subdomains. EMBO J 1990;9:1685–96.
[21] Manimaran P, Raghurami Reddy M, Bhaskar Rao T, Mangrauthia SK, Sundaram RM, Balachandran SM. Identification of cis-elements and evaluation of upstream regulatory region of a rice anther-specific gene, OSIPP3, conferring pollen-specific expression in Oryza sativa (L.) ssp. indica. Plant Reprod 2015;28:133–42. doi: https://doi.org/10.1007/s00497-015-0264-4.
[22] Manimaran P, Venkata Reddy S, Moin M, Raghurami Reddy M, Yugandhar P, Mohanraj SS, et al. Activation-tagging in indica rice identifies a novel transcription factor subunit, NF-YC13 associated with salt tolerance. Sci Rep 2017;7:1–16. doi: https://doi.org/10.1038/s41598-017-10022-9.
[23] Liu Y-G, Mitsukawa N, Oosumi T, Whittier RF. Efficient isolation and mapping of Arabidopsis thaliana T-DNA insert junctions by thermal asymmetric interlaced PCR. Plant J 1995;8:457–63. doi: https://doi.org/10.1046/j.1365-313X.1995.08030457.x.
[24] Sakai H, Lee SS, Tanaka T, Numa H, Kim J, Kawahara Y, et al. Rice annotation project database (RAP-DB): An integrative and interactive database for rice genomics. Plant Cell Physiol 2013;54. doi: https://doi.org/10.1093/pcp/pcs183.
[25] Ravikumar G, Manimaran P, Voleti SR, Subrahmanyam D, Sundaram RM, Bansal KC, et al. Stress-inducible expression of AtDREB1A transcription factor greatly improves drought stress tolerance in transgenic indica rice. Transgenic Res 2014;23:421–39. doi: https://doi.org/10.1007/s11248-013-9776-6.
[26] Schmittgen TD, Livak KJ. Analyzing real-time PCR data by the comparative CT method. Nat Protoc 2008;3:1101–8. doi: https://doi.org/10.1038/nprot.2008.73.
[27] Mangrauthia SK, Jha M, Agarwal S, Sailaja B. Delineation of gene experession pattern in rice under rice tungro virus and green lead hopper infestations. Indian J Plant Prot 2017;45:1–7.
[28] Prathi NB, Salim AP, Beena R, Achuthan VP, Abdulla NP. Morpho-physiological and proteomic analysis to identify and characterise the traditional rice genotypes for drought tolerance. Indian J Plant Physiol 2018;23:785–95. doi: https://doi.org/10.1007/s40502-018-0405-5.
[29] Bradford MM. A rapid and sensitive method for the quantitation of microgram quantities of protein utilizing the principle of protein-dye binding. Anal Biochem 1976;72:248–54. doi: https://doi.org/10.1016/0003-2697(76)90527-3.
[30] Shao J, Zhang Y, Yu J, Guo L, Ding Y. Isolation of thylakoid membrane complexes from rice by a new double-strips BN/SDS-PAGE and bioinformatics prediction of stromal ridge subunits interaction. PLoS ONE 2011;6. doi: https://doi.org/10.1371/journal.pone.0020342.
[31] Lichtenthaler HK, Wellburn AR. Determinations of total carotenoids and chlorophylls a and b of leaf extracts in different solvents. Biochem Soc Trans 1983;11:591–2. doi: https://doi.org/10.1042/bst0110591.
[32] Schonfeld MA, Johnson RC, Carver BF, Mornhinweg DW. Water Relations in Winter Wheat as Drought Resistance Indicators. Crop Sci 1988;28:526–31. doi: https://doi.org/10.2135/cropsci1988.0011183x002800030021x.
[33] Gauthami P, Subrahmanyam D, Padma V, Kiran TV, Rao YV, Rao PR, et al. Variation in leaf photosynthetic response of rice genotypes to post-anthesis water deficit. Indian J Plant Physiol 2014;19:127–37. doi: https://doi.org/10.1007/s40502-014-0086-7.
[34] Fitzgerald HA, Chern MS, Navarre R, Ronald PC. Overexpression of (At)NPR1 in rice leads to a BTH- and environment-induced lesion-mimic/cell death phenotype. Mol Plant Microbe Interact 2004;17:140–51. doi: https://doi.org/10.1094/MPMI.2004.17.2.140.
[35] Alexieva V, Sergiev I, Mapelli S, Karanov E. The effect of drought and ultraviolet radiation on growth and stress markers in pea and wheat Plant. Cell Environ 2001;24:1337–44. doi: https://doi.org/10.1046/j.1365-3040.2001.00778.x.
[36] Heath RL, Packer L. Photoperoxidation in isolated chloroplasts. I. Kinetics and stoichiometry of fatty acid peroxidation. Arch Biochem Biophys 1968;125:189–98. doi: https://doi.org/10.1016/0003-9861(68)90654-1.
[37] Dhindsa RS, Plumb-dhindsa P, Thorpe TA. Leaf senescence: Correlated with increased levels of membrane permeability and lipid peroxidation, and decreased levels of superoxide dismutase and catalase. J Exp Bot 1981;32:93–101. doi: https://doi.org/10.1093/jxb/32.1.93.
[38] Aebi H. Catalase in Vitro. Methods Enzymol 1984;105:121–6. doi: https://doi.org/10.1016/S0076-6879(84)05016-3.
[39] Castillo FJ, Penel C, Greppin H. Peroxidase release induced by ozone in Sedum album leaves. Involvement of Ca2+. Plant Physiol 1984;74:846–51. doi: https://doi.org/10.1104/pp.74.4.846.
[40] Bates LS, Waldren RP, Teare ID. Rapid determination of free proline for water-stress studies. Plant Soil 1973;39:205–7. doi: https://doi.org/10.1007/BF00018060.
[41] Yoshida S, Forno, Douglas A.Cock JH, Gomez K a. Laboratory Manual for Physiological Studies of Rice. 1976.
[42] Lakshman M. Application of conventional electron microscopy in aquatic animal disease diagnosis: A review. J Entomol Zool Stud 2019;7:470–5.
[43] Huerta-Cepas J, Capella-Gutiérrez S, Pryszcz LP, Marcet-Houben M, Gabaldón T. PhylomeDB v4: Zooming into the plurality of evolutionary histories of a genome. Nucleic Acids Res 2014;42:D897–902. doi: https://doi.org/10.1093/nar/gkt1177.
[44] Szklarczyk D, Gable AL, Lyon D, Junge A, Wyder S, Huerta-Cepas J, et al. STRING v11: Protein-protein association networks with increased coverage, supporting functional discovery in genome-wide experimental datasets. Nucleic Acids Res 2019;47:D607–13. doi: https://doi.org/10.1093/nar/gky1131.
[45] Lescot M, Déhais P, Thijs G, Marchal K, Moreau Y, Van De Peer Y, et al. PlantCARE, a database of plant cis-acting regulatory elements and a portal to tools for in silico analysis of promoter sequences. Nucleic Acids Res 2002;30:325–7. doi: https://doi.org/10.1093/nar/30.1.325.
[46] Srilatha P, Yousuf F, Methre R, Vishnukiran T, Agarwal S, Poli Y, et al. Physical interaction of RTBV ORFI with D1 protein of Oryza sativa and Fe/Zn homeostasis play a key role in symptoms development during rice tungro disease to facilitate the insect mediated virus transmission. Virology 2019;526:117–24. doi: https://doi.org/10.1016/j.virol.2018.10.012.
[47] Altschul SF, Madden TL, Schäffer AA, Zhang J, Zhang Z, Miller W, et al. Gapped BLAST and PSI-BLAST: A new generation of protein database search programs. Nucleic Acids Res 1997;25:3389–402. doi: https://doi.org/10.1093/nar/25.17.3389.
[48] Lu Y. Identification and roles of photosystem II assembly, stability, and repair factors in Arabidopsis. Front. Plant Sci 2016;7. doi: https://doi.org/10.3389/fpls.2016.00168.
[49] Jeong D-H, An S, Kang H-G, Moon S, Han J-J, Park S, et al. T-DNA insertional mutagenesis for activation tagging in rice. Plant Physiol 2002;130:1636–44. doi: https://doi.org/10.1104/pp.014357.
[50] Reddy M, Reddy S, Manimaran P, Quadriya H, Mahendranath G, Km B, et al. Development of Activation Tagged Mutants in Rice CV BPT 5204 and Identification of the SUMO Protease Gene Associated with Early Flowering. J Rice Res 2017;10:46–51.
[51] Dastur RH, Desai BL. The relation between water-content, chlorophyll-content, and the rate of photosynthesis in some tropical plants at different temperatures. Ann Bot 1933:69–88. doi: https://doi.org/10.1093/oxfordjournals.aob.a090378.
[52] Eaton SV. Chlorophyll Content and Photosynthesis. Bot Gaz 1931;91:223–4. doi: https://doi.org/10.1086/334147.
[53] Murchie EH, Lawson T. Chlorophyll fluorescence analysis: A guide to good practice and understanding some new applications. J Exp Bot 2013;64:3983–98. doi: https://doi.org/10.1093/jxb/ert208.
[54] Long SP, Humphries S. Photoinhibition of photosynthesis in nature. Annu Rev Plant Physiol Plant Mol Biol 1994;45:633–62.
[55] Ruban AV. Quantifying the efficiency of photoprotection. Philos Trans R Soc B Biol Sci 2017;372. doi: https://doi.org/10.1098/rstb.2016.0393.
[56] Duan Q, Jiang W, Ding M, Lin Y, Huang D. Light affects the chloroplast ultrastructure and post-storage photosynthetic performance of watermelon (Citrullus lanatus) plug seedlings. PLoS ONE 2014;9. doi: https://doi.org/10.1371/journal.pone.0111165.
[57] Nishiyama Y, Allakhverdiev SI, Murata N. Protein synthesis is the primary target of reactive oxygen species in the photoinhibition of photosystem II. Physiol Plant 2011;142:35–46. doi: https://doi.org/10.1111/j.1399-3054.2011.01457.x.
[58] Wang T, Li S, Chen D, Xi Y, Xu X, Ye N, et al. Impairment of FtsHi5 Function Affects Cellular Redox Balance and Photorespiratory Metabolism in Arabidopsis. Plant Cell Physiol 2018;59:2526–35. doi: https://doi.org/10.1093/pcp/pcy174.
[59] Bhattacharjee S. ROS and Regulation of Photosynthesis. React. Oxyg. Species Plant Biol., Springer India 2019:107–25. doi: https://doi.org/10.1007/978-81-322-3941-3_5.
[60] You J, Chan Z. Ros regulation during abiotic stress responses in crop plants. Front Plant Sci 2015;6:1092. doi: https://doi.org/10.3389/fpls.2015.01092.
[61] Gong Z, Dong CH, Lee H, Zhu J, Xiong L, Gong D, et al. A DEAD box RNA helicase is essential for mRNA export and important for development and stress responses in Arabidopsis. Plant Cell 2005;17:256–67. doi: https://doi.org/10.1105/tpc.104.027557.

[62] Gong Z, Lee H, Xiong L, Jagendorf A, Stevenson B, Zhu JK. RNA helicase-like protein as an early regulator of transcription factors for plant chilling and freezing tolerance. Proc Natl Acad Sci U S A 2002;99:11507–12. doi: https://doi.org/10.1073/pnas.172399299.
[63] Yang Y, Sornaraj P, Borisjuk N, Kovalchuk N, Haefele SM. Transcriptional Network Involved in Drought Response and Adaptation in Cereals. Abiotic Biot Stress Plants - Recent Adv Futur Perspect 2016:3–30. doi: https://doi.org/10.5772/62336.
[64] Rathinasabapathi B. Metabolic Engineering for Stress Tolerance: Installing Osmoprotectant Synthesis Pathways. Ann Bot 2000;86:709–16. doi: https://doi.org/10.1006/anbo.2000.1254.
[65] Xiao K, Mao X, Lin Y. Trichome, a Functional Diversity Phenotype in Plant. Mol Biol 2016. doi: https://doi.org/10.4172/2168-9547.1000183. s1:1–6.
[66] Agarie S, Agata W, Uchida H, Kubota F, Kaufman PB. Function of silica bodies in the epidermal system of rice (Oryza sativa L.): testing the window hypothesis. J Exp Bot 1996;47:655–60. doi: https://doi.org/10.1093/jxb/47.5.655.
[67] Lawson T, Blatt MR. Stomatal size, speed, and responsiveness impact on photosynthesis and water use efficiency. Plant Physiol 2014;164:1556–70. doi: https://doi.org/10.1104/pp.114.237107.
[68] Fan X, Wu J, Chen T, Tie W, Chen H, Zhou F, et al. Loss-of-function mutation of rice SLAC7 decreases chloroplast stability and induces a photoprotection mechanism in rice. J Integr Plant Biol 2015;57:1063–77. doi: https://doi.org/10.1111/jipb.12350.
[69] Okada K, Inoue Y, Satoh K, Katoh S. Effects of light on degradation of chlorophyll and proteins during senescence of detached rice leaves. Plant Cell Physiol 1992;33:1183–91. doi: https://doi.org/10.1093/oxfordjournals.pcp.a078372.
[70] Talla SK, Panigrahy M, Kappara S, Nirosha P, Neelamraju S, Ramanan R. Cytokinin delays dark-induced senescence in rice by maintaining the chlorophyll cycle and photosynthetic complexes. J Exp Bot 2016;67:1839–51. doi: https://doi.org/10.1093/jxb/erv575.
[71] Skirycz A, de Bodt S, Obata T, de Clercq I, Claeys H, de Rycke R, et al. Developmental stage specificity and the role of mitochondrial metabolism in the response of Arabidopsis leaves to prolonged mild osmotic Stress. Plant Physiol 2010;152:226–44. doi: https://doi.org/10.1104/pp.109.148965.
[72] Chen JH, Chen ST, He NY, Wang QL, Zhao Y, Gao W, et al. Nuclear-encoded synthesis of the D1 subunit of photosystem II increases photosynthetic efficiency and crop yield. Nat Plants 2020. doi: https://doi.org/10.1038/s41477-020-0629-z.